CHAPTER 4: RESULTS OF FLOW FORMING

In the previous chapters, the design and fabrication of the experimental setup have been discussed and in the last chapter, a mathematical model has been proposed to calculate the flow forming forces. The present chapter presents the results of the flow forming for Al6101 T6, Al7075 and Al2014 samples. The chapter is divided into three different sections. The first section presents the results of flow forming for Al6101 T6 samples. The second section presents the results of flow forming for Al7075 samples. Finally, the last section of this chapter presents the results of flow forming for Al2014 samples.

4.1 Results of flow Forming of Al6101

A total of 5 samples have been flow formed under various conditions. Figure 4.1 shows the flowformed Al6101 samples. The samples are named as FF01, FF02, FF03, FF04 and FF05.

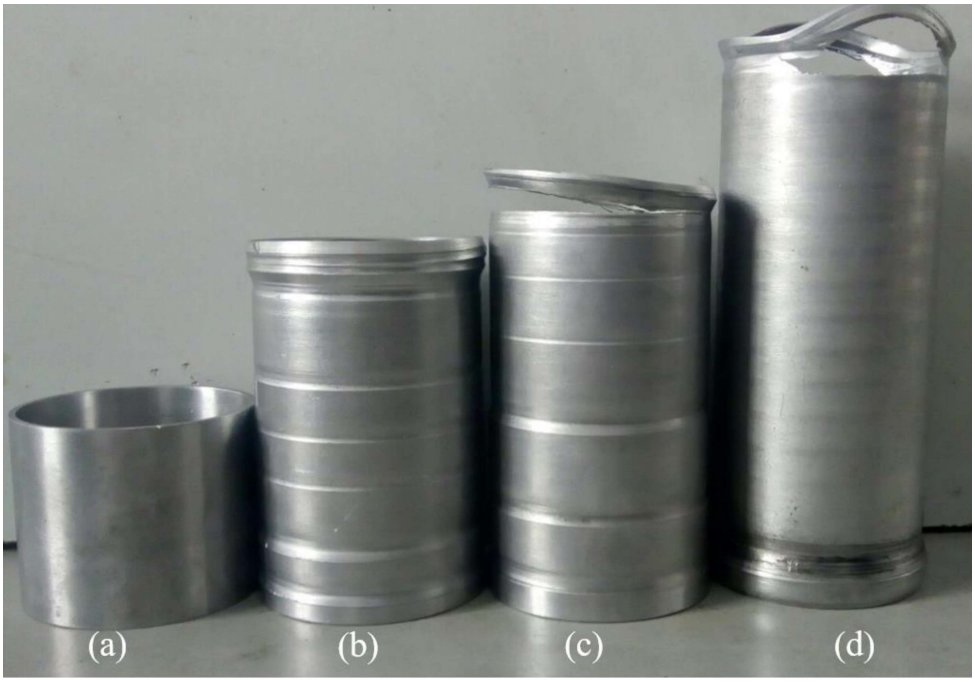

Figure 4.1: Al6101 samples (a) Preform (b) FF02 (c) FF01 (d) FF03

4.1.1 Thickness reduction

FF01 represents the stepped cylinder formed in multipass flow forming. The different steps have been marked as IA to IE as shown in Figure 4.2. IA region maximum deformed region while IE refers to an undeformed region. The intermediate regions are marked as ID to IB from less deformed to more deformed regions.

The flow formed jobs were then cut longitudinally to measure the thickness variation in different regions. Within each region, the thickness was measured at five different points, away from the end, to avoid the roller marks present at start of the pass and end of the pass. The average thickness has been calculated for each region and was used for thickness reduction evaluation.

The percentage thickness reduction is calculated as

$$\%TR = \frac{r_0 - r_f}{r_0} \tag{4.1}$$

Where %TR is percentage thickness reduction, r_0 is intial thickness and r_f is the final thickness

During the process, the maximum and minimum thickness reduction was found to be 58.3 % and 8 % respectively. The thickness of the preform was reduced from the initial 2.6 mm to 1 mm in 4 steps. The regions are marked as 1A to 1E, where 1A involved a maximum thickness reduction of 58.3 % while 1D involved a minimum thickness reduction of 8 %. 1E represents the starting region which is not flow formed. Figure 4.2 summarizes the incremental thickness reduction per pass and the cumulative thickness reduction in the region.

Figure 4.2: The preform and the flow formed product showing the different regions. IE represents the initial region (not flow formed) while regions 1A-1D denote the thickness reduction obtained in 4 different passes

.

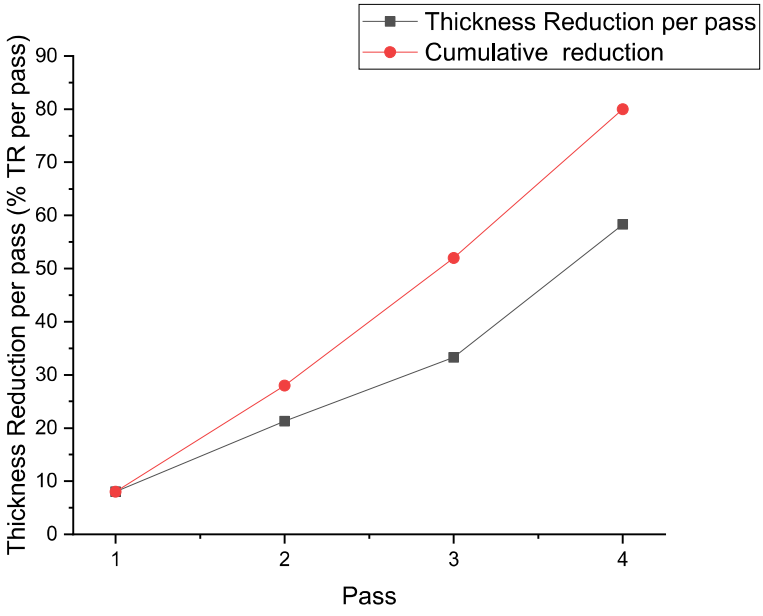

Figure 4.3: Thickness reduction per pass and cumulative thickness reduction. Pass 1 refers to 1D, pass 2 refers to region 1C and so on. Pass 4 refers to 1A

4.1.2 Temperature Variation

The temperature was measured using non-contact infrared thermometer. The temperature has been found to increase during the process mainly due to loss of energy as heat. However, change in temperature is found to be less than 30°C during the flow forming operation. The maximum temperature reached was 50-55°C while the ambient temperature was 27°C. This can be due to the high thermal conductivity of aluminium perform. Also, the time taken for each pass was less than 50 seconds and so sufficient time for temperature built up was not available.

4.1.3 Radial force, circumferential force, and axial force

During flow forming, the material flows in the gap between the mandrel and the roller. As a result, the material flows mainly in the axial direction and the circumferential direction. During the axial movement of the roller, the material gets stretched and compressed due to the roller attack angle. As a result, both tensile and compressive stresses are generated. As the roller deforms the material, an opposite reaction force is exerted on the roller by the deforming material which results in two types of forces- the axial force and the circumferential force. The radial force arises mainly due to compressive forces due to roller in-feed motion.

Figure 4.4 to Figure 4.6 shows the variation of radial forces, circumferential forces, and axial forces respectively, at different percentage thickness reduction, to the time of completion of one individual pass.

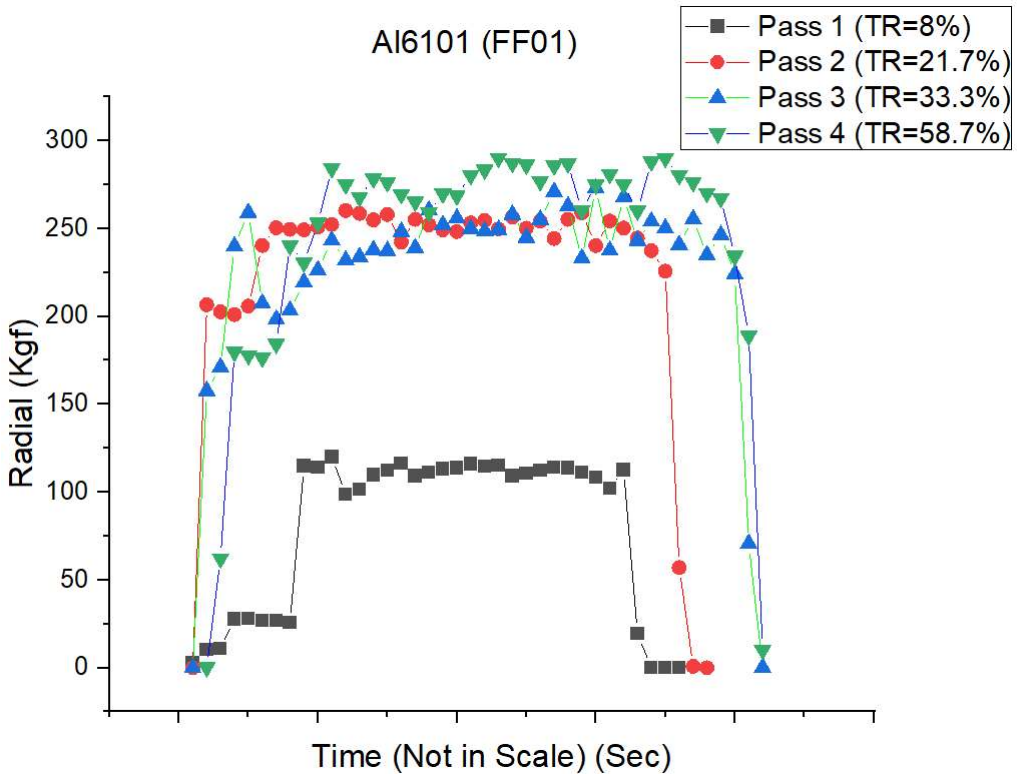

Figure 4.4: Variation of radial force during flow forming operation of sample FF01

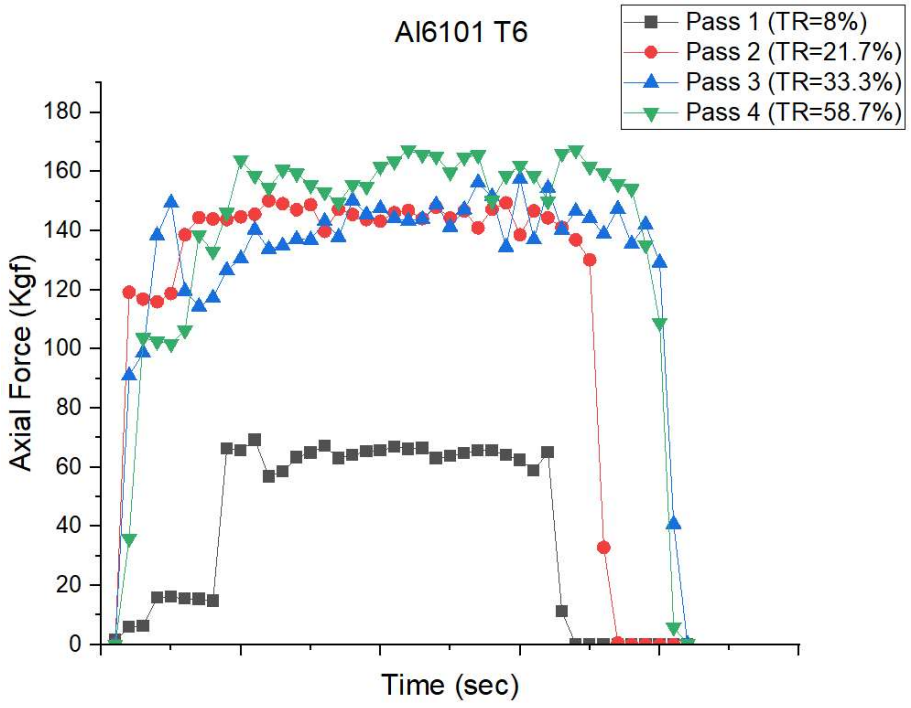

Figure 4.5: Variation of axial force during flow forming operation of sample FF01

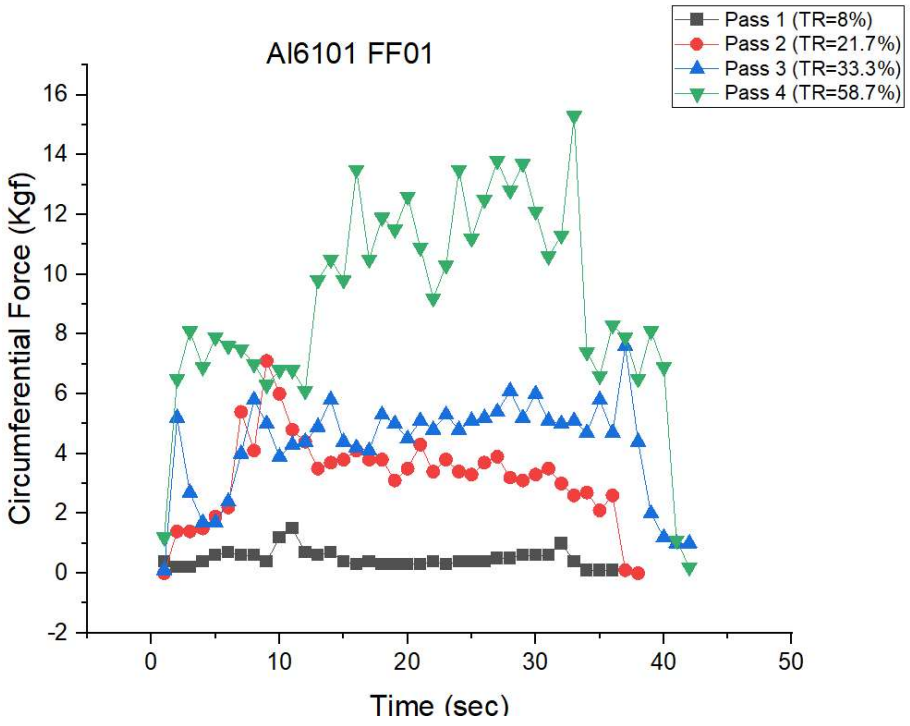

Figure 4.6: Variation of circumferential force during flow forming operation of sample FF01.

It can be seen from Figure 4.4 to Figure 4.6, all the components of the flow forming forces that is, axial forces, the circumferential forces, and the radial forces is found to increase with the increase in percentage reduction. This can be explained on the basis that as the percentage reduction increases, the amount of material deforming and flowing along the radial and circumferential direction increases. As a result, the reaction forces on the roller increases, and hence the magnitude of each of the forces increases.

The radial force is found to be most significant in the flow forming process. Under the present experimental condition, the radial force was found to be more uniformly increasing, as compared to radial or circumferential force. The average magnitude of axial force is found to increase from 141.5 kgf at %TR=8 to 293.5 kgf at %TR=58.3%. However, the peak values observed in the investigation was found to be 310.2 kgf at %TR of 58.3%.

Table 4.1 summarizes the mean radial, mean circumferential, and mean axial force in each pass. The mean data is taken when the measured force data have been stabilized. The data points at the start and the end of the trial have not been considered to avoid the data fluctuations related to sudden removal and engagement of roller.

Table 4.1: Summary of mean radial force, mean circumferential force and mean axial force variation in each pass

Pass	%TR Per pass (%)	Mean Circumferential Force (kgf)	Mean Axial force (kgf)	Mean Radial Force (kgf)
1 (1D)	8	0.5	16.9	141. 5
2 (1C)	21.3	3.5	41.5	240.1
3 (1B)	33.3	4.4	44.6	276. 2
4 (1A)	58.3	9.7	49.5	293.5

The axial force is found to increase as the cumulative percentage thickness reduction %TR has increased from 8 % in the first pass to 58.3 % in the last pass. However, the average radial force has been found to increase in an irregular order. Further, in the last three passes, the axial force just increased by about 17.3 kgf even though %TR was 58.5 % in that passes. A similar variation is also observed in the case of circumferential force and axial force. The magnitude of axial force is found to be intermediate between the magnitude of the circumferential force and the radial force. This has been reported by other authors. [28],[29],30][31],[32].

The radial force is found to be most significant in the flow forming process. Under the present experimental condition, the radial force was found to be more uniformly increasing, as compared to radial or circumferential force. The average magnitude of axial force is found to increase from 141.5 kgf at %TR=8 to 293.5 kgf at 58.3 kgf. However, the peak values observed in the investigation was found to be 310.2 kgf at %TR of 58.3%.

From it is clear that circumferential force in general increases with an increase in thickness reduction. However, the magnitude of the force is much smaller than that axial or radial component. The circumferential force was about 9.7 kgf when the maximum % TR was 58.3 %.

The measured forces in all three directions indicate that the force not only increases with increaing thickness reduction but also on the number of prior passes it had already undergone and the thickness of the workpiece in that pass.

It can be observed that the axial force increased by almost 69.68% from 141.5 kgf to 240.1 when the %TR increased from 8% to 21.3 %. However, the increase in axial force was increased from 240.1kgf to 293.5 kgf when %TR increased from 21.3% to 58.3%. an increase of 22.2% in force. This showed that the strain hardening in Al6101 during the process is not high. Further, there may be some thermal softening due to temperature increase during the process.

Flow forming forces in FF02 (stepped cylinder)

In flow forming of FF02, the process parameters used in the investigation are summarized in Table 4.2. The process parameters are chosen such that the parameters can be directly compared with the results of sample FF01.

Table 4.2: Process Parameter for FF02

Process Parameters for FF02				
Intial thickness 2.0 mm		Mandrel Rpm = 420	Feed rate : 0.04mm/rev	
	Pass 1	Pass2	Pass 3	Pass 4
Infeed (mm)	0.1	0.1	0.2	0.1
% thickness reduction	20	25	33.3	40

This was done to ensure that the tube can be elongated to a much longer length without failure with increasing hardness in subsequent steps. The feed rate was kept same as FF01 while the mandrel rpm was increased to 420 rpm.

Figure 4.7: Flow formed FF02-Multistep flow formed sample (a) preform (b) Flow formed product.

During the investigation, FF01 was found to crack from the end while in flow forming of sample FF02 no crack was observed. The force in FF02 in subsequent steps and the thickness reduction were summarized in Table 4.3.

Table 4.3: Thickness reduction and Average flow forming Forces in FF02

Pass	Thickness Reduction(%)	Average Radial force (kgf)	Average Axial force (kgf)	Average Circumferential force (kgf)
1st	20	150.1	82.5	2.1
2nd	25	158.9	83.6	3.0
3rd	33.4	168.2	97.2	3.3
4rd	40	180.4	101.9	3.9

Table 4.4 shows the thickness reduction in flow forming of FF03, FF04, and FF05. The sequence of steps followed was to provide infeed of 0.2mm in each passes in FF03 and FF04. However, the mandrel rpm was kept at 420 rpm but feed rate in forming FF03 was 0.06mmm for first passes and 0.12mm for region II for next passes in region II . FF04 was deformed in single pass at 420 rpm, 0.04 mm/rev and infeed of 0.4mm.

Table 4.4: Thickness reduction and average flow forming forces in FF03, FF04 and FF05

Passes	Final Thickness Reduction (%)	Max Radial force (kgf)	Max Axial force	Max Circumferential force (kgf)
FF03	80	163.5	95.2	7.8
FF04	20 (region I); 80 (region II)	115.7 159.7	59.3 92.2	2.6 5.6
FF05	40	153.5	87.9	3.4

It is clear from the values that similar to the results for FF01 and FF02, the average circumferential forces during flow forming of samples FF03 to FF05 ,are found to least while the radial forces are found to be the most significant. Like in FF01, the forces increase with an increase in thickness reduction. The increase is found to be more significant in FF05 where the thickness reduction was about 40% percentage in single pass. The increase in forces for flow formed sample FF05, shows that the magnitude of forces depends not only on thickness reduction but also on initial thickness. For the same thickness reduction per pass, the forces are found to be more for higher thickness. This can be explained as the thickness increases for the same thcikness reduction, higher volume of material would be deformed. So the magnitude of forces would be higher.

Figure 4.8: Preform and Flow formed FF03

Samples FF03, FF04, and FF05 were flow formed in multipass with different feed rates. Figure 4.8 shows the FF03 and the size of the preform used. The material was deformed

uniformly. Lubrication was done with diesel oil which was intermittently done at the roller workpiece contact zone. External lubrication at roller workpiece performed three functions First, it reduces friction at the contact region, Secondly, it flushes out any chip formed which is necessary for good surface finish and third, it would prevent local heat buildup.

The material flow during flow forming of sample FF03 was found to be unform and resulted in a surface with surface finish with Ra of 0.43 μm.

In FF04, the preform was divided into two different zones with the varying feed rate of 0.06mm per revolution and a feed rate of 0.12mm per revolution. The mandrel speed was kept constant at 420 rpm. The average forming forces are given in Table 4.4. The average values of radial, axial and circumferential components of forces shown increasing trend with increasing feed. The average radial force has increased from 115.7 kgf in first region to 127.8kgf in first pass of second region with similar thickness reduction, keeping mandrel speed same. Some irregularity in material flow is observed in between the zone. This can be due to two factors- first, due to entrance defect which was due to unstable flow when a roller pushes a rotating mandrel. Secondly, the tendency of backward flow that occurred during the deformation of the second zone.

The surface finish in region I is found to have Ra value of 1.02μm which is found to be better than surface finish in region II which has Ra value of 3.59 μm has been found to deteriorate due to increasing roller marks.

Figure 4.9: Flow formed samples FF04 and FF05

4.1.4 Thickness Variation

In the stepped flow formed product, the average thickness along each step section was measured to identify the uniformity of the operation. The measurement showed that the thickness was uniform in the middle section of each step. However, near the end and start of each section, the variation was large. Presence of wrinkles, non –uniform zone near the intermediate steps causes problem of thickness variation problem.

4.1.5 Diametral growth

The diametral growth is found in almost all flow formed samples. The diametral growth, in general has been found to be higher in regions of higher thickness reduction. . The diametral growth in FF05 was also around 1.6mm at the end of the tube. However, the defect is more pronounced in 1C of FF01 than IA, which represents a region of maximum deformation. This can be attributed to residual stresses that are induced during the process. The residual stress analysis was done for samples cut out from region IA and IC. The

residual stress test was done on Panalytical MRD System at IIT Bombay. The residual force in the IC region of FF01is found to be -38.2 ± 1.5 MPa while in IA region of sample FF01, the residual stress is found to be $+1.6 \pm 2.7$ MPa. The presence of higher residual stress would be probable factor for increase in diametral factor.

4.1.6 **Ovality**

Ovality is a common problem which arises due to no uniform flow. The problem of the ovality is found to be more in FF06 in which initial thickness reduction was large. The defect is less when the thickness reduction was increased gradually in a stepped job as in FF01 and FF02. Further, in FF03 ovality is found to be less. In FF04, the ovality is found to be higher when feed rate was increased from 0.06mm/rev to 0.12 mm/ rev. The problem of ovality is also found to be related with the point of exit of roller after the flow forming operation. During forming of FF03, the problem of ovality was encountered in individual passses but the amount of ovality was not uniform. This would probably be related to relative path of interaction between the roller and the workpiece. In the present investigation, only one roller was used. The relative motion between the roller and workpiece would follow a helical path. The point where the roller is withdrawn after the completion of the passes would be endpoint of the helix that would be definitely be more stretched than its diametrically opposite point.

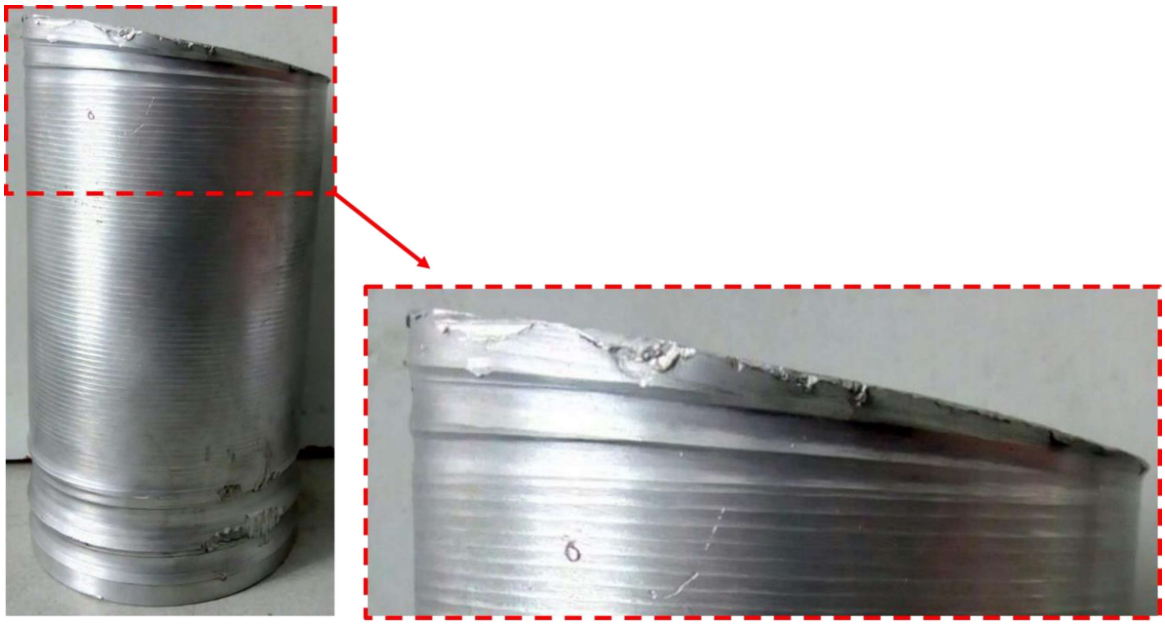

(a) (b)

Figure 4.10: Ovality in FF05 (a) Flow formed Sample FF05 (b) enlarged view of the end section

4.1.7 **Surface Roughness:**

Surface roughness has been measured on Mitutoyo Surftest(SV-2100S4) present in metrology lab of production engineering. The surface roughness of the outer surface of mandrel, surface of roller surface, and the inner surface of flow formed product is shown in Table 4.5.

In FF04, the surface roughness of inner surface of region with higher feed rate is found to be higher as compared to be higher. The outer surface is found to have more surface roughness as compared to inner surface especially at the start and the end of the flow forming pass. The surface finish has been found to be deteriorated in regions where amount of back flow has taken place. In sample FF04, the surface roughness of inner and outer surface is found to be higher. Roller marks were present on outer surface and roller impressions are also seen.

Table 4.5: Surface roughness measurement

Srl No.	**Ra (mean Value) μm**
Mandrel Roughness	0.286
Roller Roughness	0.546
Undeformed Al6101 preform	0.586
FF01	0.746
FF02	0.663
FF03	0.495
FF04	1.01
FF05	0.721

Presence of roller marks and wrinkling at the start, makes the surface more rough. Only surface roughness at some areas of uniform deformation was measured. The result showed that an average Ra of 0.962 μm was found in IA region of FF01. Similarly, for FF05, the surface was having lot of roller marks. As a result the surface roughness was higher with Ra value of 8.645μm. Overall, the results show that the product surface finish would be decided by the surface roughness of the roller and that of surface. Further, the surface finish improves as the process becomes more uniform as in case of FF03.

4.1.8 **Microhardness Variation:**

The microhardness of the preform and flow formed product was measured on Vickers microhardness tester (model – SEMIAUTOMATIC, serial no.-104, MICROMACH Technologies, Pune) Vickers diamond indenter at an applied of 50g for a dwell time of 10 s. The hardness values in different regions of FF01 are shown in Figure 4.11

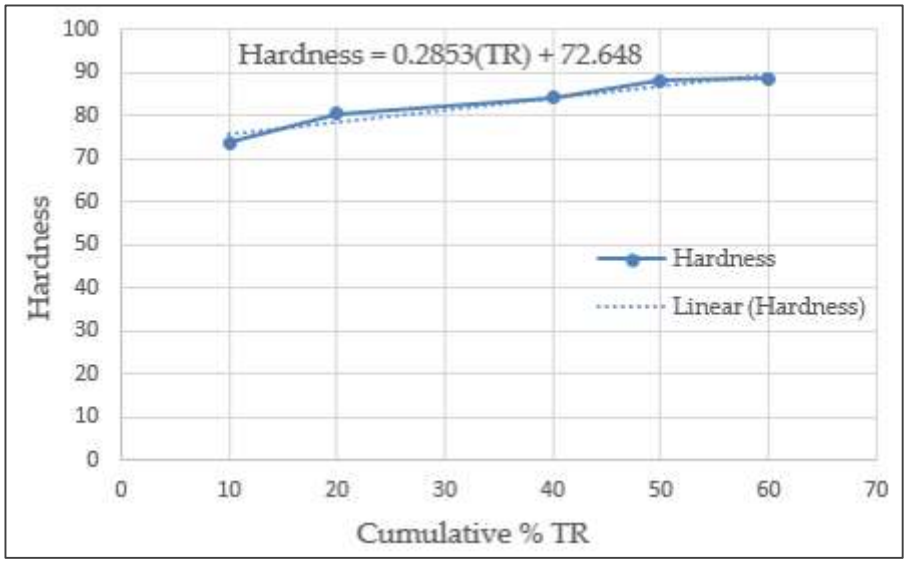

Figure 4.11: Variation of Vickers hardness with cumulative percentage thickness reduction.

The measured hardness showed a continuous increase with an increase in thickness reduction. The average hardness in FF01 increased by 73.59 HRC in region 1E to 88.46 HRC in region 1A. The increase in hardness can be explained based on strain hardening. As thickness reduction increases per pass, the amount of plastic strain increases, and therefore the workpiece gets hardened for the successive pass. The variation of hardness with cumulative hardness is shown in table 4.6

A mathematical relationship for Al6101 relating Vickers hardness and cumulative hardness was obtained based on the data.

Table 4.6: Hardness variation in different sections of FF01

Region	Readings taken	Hardness	Mean value	Standard Deviation
1A	1	90.64	88.46	1.95
	2	86.43		
	3	89.52		
	4	87.25		
1B	1	89.52	87.985	1.26
	2	87.56		
	3	88.32		
	4	86.54		
1C	1	87.28	84.1075	2.48
	2	81.38		
	3	83.21		
	4	84.56		
1D	1	77.79	80.45	2.46
	2	81.38		
	3	83.4		
	4	79.23		
1E	1	69.4	73.59	3.36
	2	76.26		
	3	76.35		
	4	72.35		

4.1.9 Tensile Test

Tensile specimen was cut from the flow formed the samples. As the thickness of the flow formed samples were around 0.4 mm, hence miniature samples were prepared based on Barba's law.

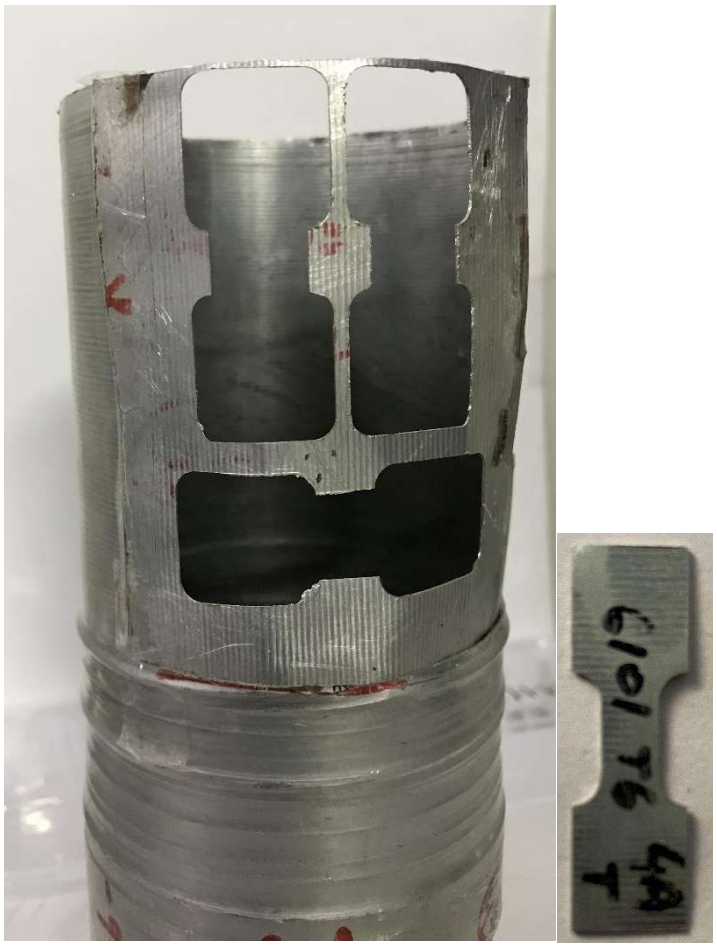

(a) (b)

Figure 4.12: (a) Tensile specimen cut out from flow formed FF04. (b) One Tensile specimen

The tensile specimen was cut from the flow formed samples using a CNC machine. The tensile specimen was tested was cut in the lateral and transverse direction. The dimensions of the tensile specimen were decided based on Barba's Law (Appendix 2). The testing was done on M/s Instron_Universal Testing Machine (Model/Supplier: Instron-1195) with

crosshead velocity of 0.025 mm/min. The results of the tensile test of FF04 is shown in Figure 4.13.

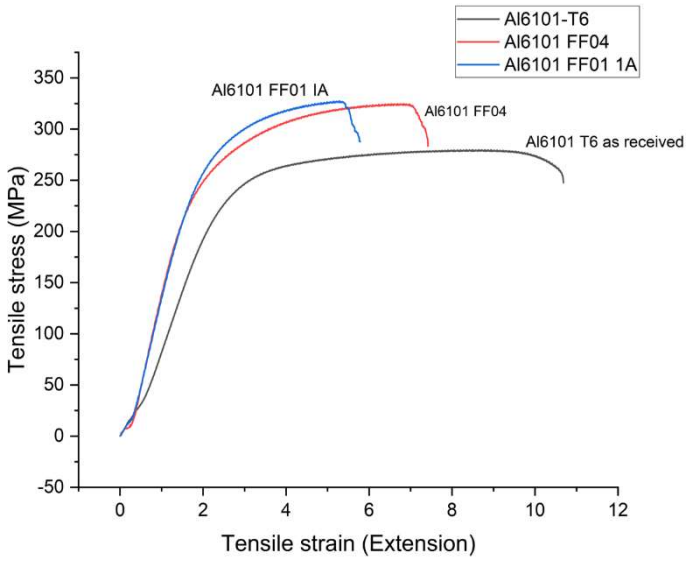

Figure 4.13: Engineering Stress- engineering strain curve of sample FF04

The tensile stress at yield (0.2% offset) was found to be 248.03 MPa while the ultimate tensile strength was found to be 276.5 MPa and the elongation was found to be 10.64%.

4.1.10 **XRD plots:**

Phases were characterized by Rigaku Miniflex X-ray diffractometer with Cu (Kα) radiation within the angular range(2θ) of 30º- 80º at the scan rate of 5º/min The XRD plot are shown in Figure 4.14. The diffraction pattern shows high intensity peaks for $\alpha - Al$. Small intensity peaks of Mg_2Si (β') intermetallics. The presence of β' intermetallics has been reported other authors .[86], [87] . The presence of Mg_2Si (β') is common in Al-Mg-Si alloys.

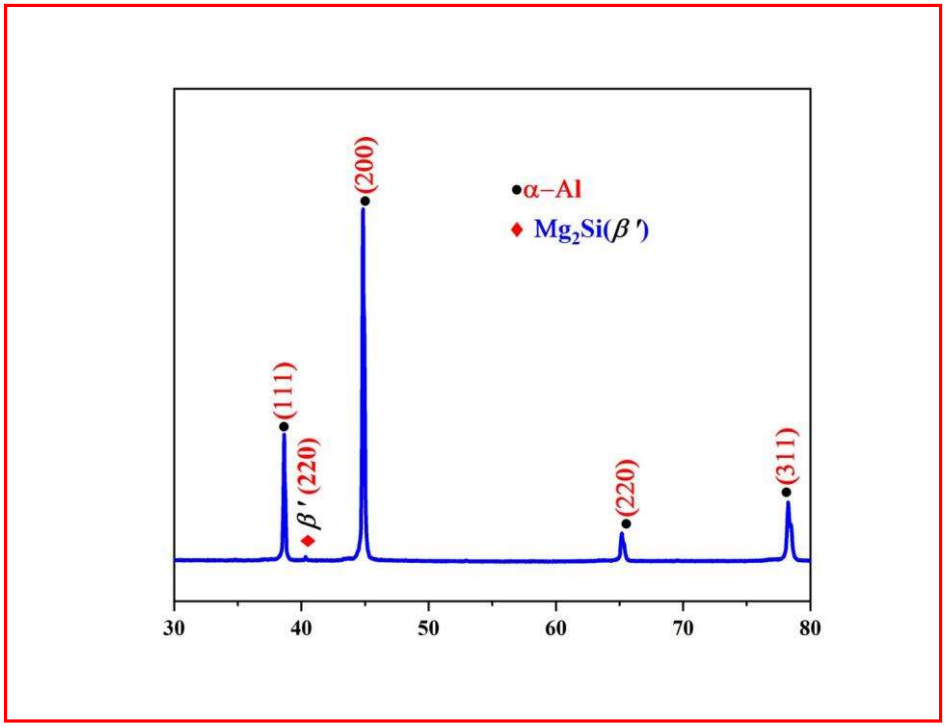

Figure 4.14: X-ray diffraction pattern of as received 6101 T6 Al alloy.

The X-ray diffraction pattern of flow formed workpiece is shown in Figure 4.15. As seen from the XRD pattern, the intensity of (111) has increased on flow forming while the intensity of (200) decreases. This shows that the slip has taken place along (111) plane.

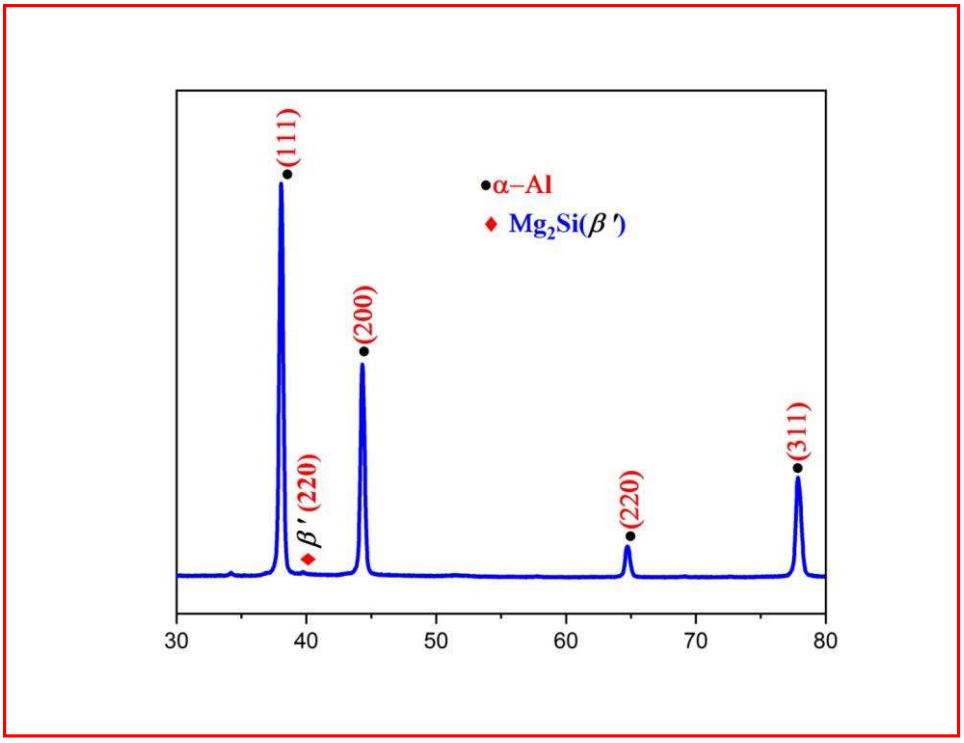

Figure 4.15: X-ray diffraction of flow formed sample.

Crystallite size (D_{hkl}) and residual lattice microstrain (e_{hkl}) are determined on the major XRD peaks individually of α-Al, (111), (220), (311) planes from the corrected Lorentzian and the Gaussian components of integral breadth widths.

On calculation, the crystallite size decreased from 9.62 Å to 5.11Å . However, the lattice microstrain (%) was found to increase from 13.27 to 18.60 and the dislocation density was found to increase from 46 X10^{17} /m^2 to 102.38 X10^{17} /m^2.

4.1.11 **EBSD Analysis :**

The EBSD analysis was done on undeformed preform and flow formed samples. Samples were mechanically polished by abrasive papers up to P2000, then cloth polished using alumina sol. The samples were electro polished and then tested for EBSD analysis. Figure 4.16 shows the inverse pole figure map of undeformed Al6101 preform.

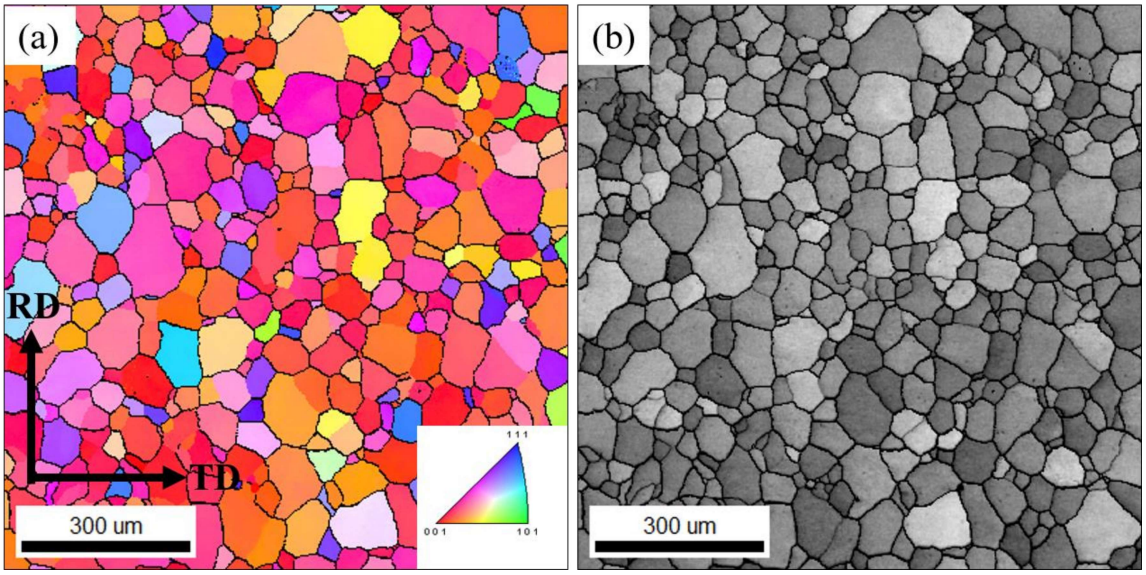

Figure 4.16: EBSD result of preform Al6101. (a) Inverse pole figure map (b) Image quality map

Figure 4.16 shows that most of the crystal are oriented in [001] direction. Table 4.7 shows the grain size distribution in undeformed samples. The grain size were found to be slightly coarser with grain size of 66.7121 μm was found to have highest area fraction (Table 4.7).

Table 4.7: Grain Size distribution in Preform Al6101

Chart: Grain Size (diameter)

Edge grains included in analysis

Diameter [microns]	Area Fraction
2.46925	6.04106e-05
3.03419	2.33847e-05
3.72838	9.74365e-06
4.58139	0.000124719
5.62957	7.40517e-05
6.91755	0.000228001
8.50022	0.000806774
10.445	0.00129201
12.8347	0.00129785
15.7711	0.00537849
19.3794	0.00892518
23.8132	0.0133936
29.2614	0.0304918
35.956	0.0598942
44.1824	0.0917267
54.2909	0.155986
66.7121	0.205523
81.9751	0.175238
100.73	0.178122
123.776	0.0714053

Summary Statistics [microns]

Average:	
Number	42.4428
Area	71.9922
Standard Deviation:	
Number	26.7599
Area	27.4738

The EBSD analysis of flow formed sample FF01 is shown in Figure 4.17. The sample was taken from IA region of the sample.

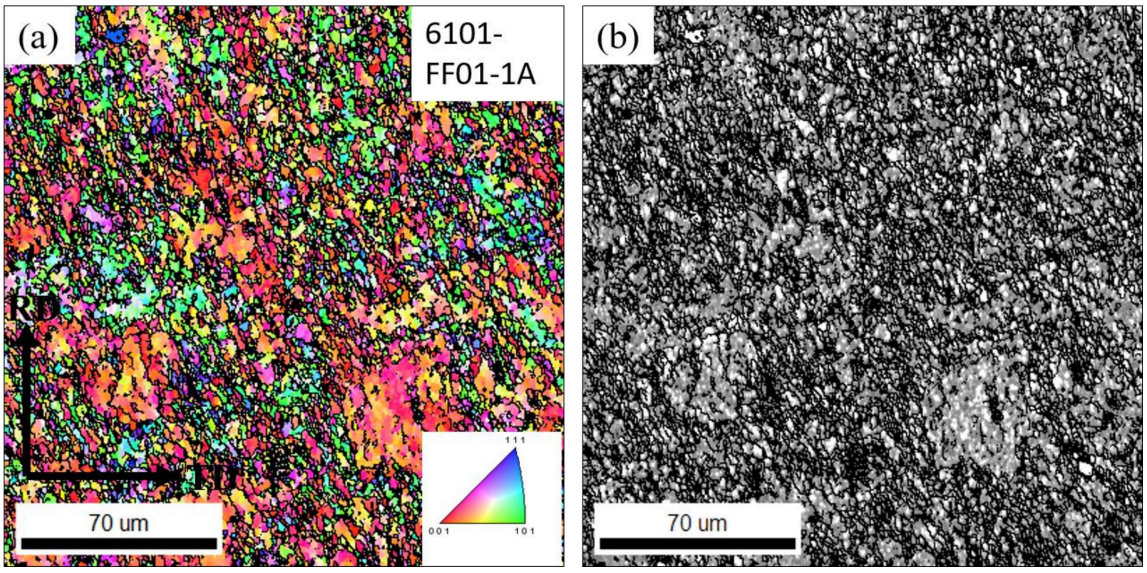

Figure 4.17: EBSD result of flow formed Al6101 FF01 IA (a) Inverse pole figure map (b) Image quality map

The EBSD analysis of flow formed sample that is taken from IA region of FF01 shows fine grain size structure as compared to the undeformed structure. More grains are found to be oriented in <101> direction which is the characteristic slip direction of FCC crystals.

The grain distribution shows that grain size of 2.1963 μm was found to have the highest area fraction. This shows significant grain refinement as compared to the undeformed samples that showed grain of diameter 66.7121 μm having the maximum area fraction.

Table 4.8: Grain size distribution in flow formed FF01 IA

Chart: Grain Size (diameter)

Edge grains included in analysis

Diameter [microns]	Area Fraction
0.441048	0.000772955
0.539061	0.00310266
0.658855	0.0049014
0.80527	0.00954816
0.984223	0.0266254
1.20294	0.0611538
1.47027	0.103419
1.79701	0.137277
2.19635	0.171175
2.68444	0.151508
3.28099	0.103657
4.01012	0.0790166
4.90127	0.0603934
5.99047	0.0384256
7.32171	0.0116232
8.94879	0.0179206
10.9375	0.00841763
13.3681	0
16.3388	0
19.9697	0.0110616

Summary Statistics [microns]

Average:	
Number	1.66659
Area	3.05909
Standard Deviation:	
Number	0.919559
Area	2.65152

The grain distribution shows that grain size of 2.1963 μm was found to have the highest area fraction. This shows significant grain refinement as compared to the undeformed samples that showed grain of diameter 66.7121 μm having the maximum area fraction. Figure 4.18 shows the misorientation angle of undeformed and flow formed samples.

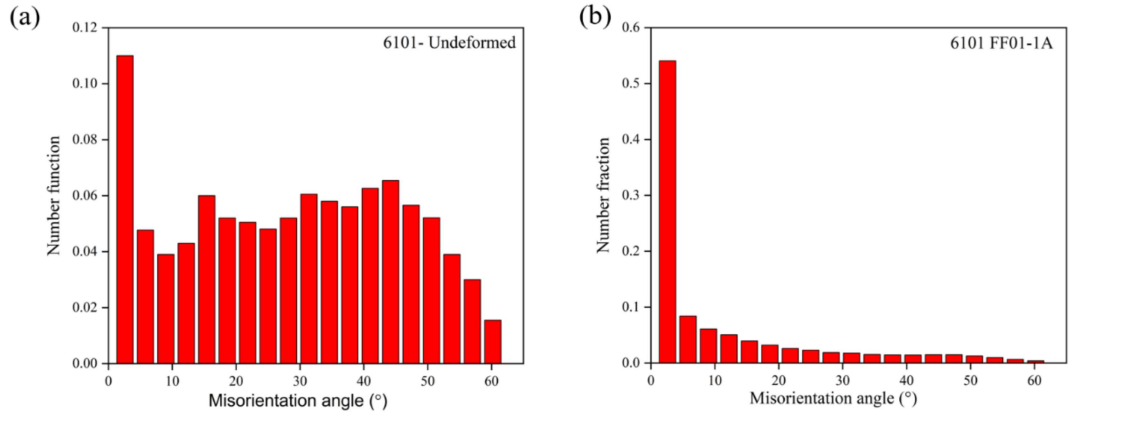

Figure 4.18: (a) Misorientation angle in undeformed samples (b) Misorientation angle in flow formed samples FF01 IA.

Based on misorientation angle data, the grain boundary can be classified as high angle grain boundary (HAGB) if the Misorientation angle is greater than 15º .while if the Misorientation angle is less than 15º, then it is regarded as low angle grain boundary (LAGB). The misorientation angle analysis data shows the presence of a large portion of high angle grain boundaries in undeformed samples while the high angle grain boundaries are very few. Low angle grain boundaries are characteristics of cold formed product [88][89][90].

4.1.12 **Defect Analysis**

All samples of Al6101 T6 showed elongation 2-3 times without failure. No crack was observed in the flow-formed product. However, other defects that were frequent were diametral growth, roller mark, wrinkling, ovality, and uneven undulations at the start and end of the product.

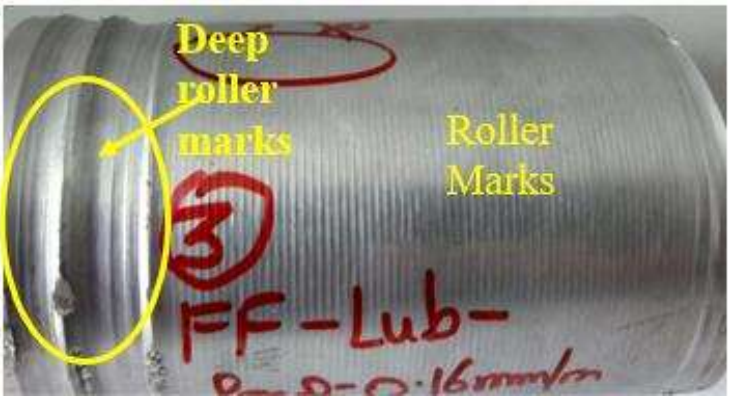

Figure 4.19: Defects in flow formed Al6101sample FF05

The figure shows the roller mark on the surface. The roller marks is found to be highest in case of sample FF05 shown in Figure 4.19. The feed rate in case of FF05 was 0.16mm/rev. This shows that the defect of roller marks increases with increase in the feed rate of the roller. The presence of deep roller marks is due to removal of the roller from the end of the pass. The roller was withdrawn before the end to prevent any crack formation as the material flow was found to be non-uniform near the end in the trial runs.

4.2 Results of Flow forming of Al7075

This section presents the results of the flow forming of Al7075. Five samples were flow formed under different conditions.

Table 4.9: Chemical composition of Al7075

Si	Fe	Cu	Mn	Mg	Cr	Zn	Ti	Al
0.3	0.38	1.1	0.1	2.4	0.21	5.4	0.0.1	Remaining

Table 4.10: Heat-treated Condition of samples of 7075

Heat Treated	T6 temper
7075-F3, 7075-F4, 7075-F5	7075-F1, 7075-F2,

4.2.1 Geometrical Characteristics

The initial dimension of the preform and the final dimensions of the product is shown in Table 4.11. The flow formed T6 samples 7F01 and 7F02 did not show any appreciable increase in length. The thickness of the end portion of the product was found to be thinner than the rest portion showing the non-uniform deformation. It was observed that there was slipping of the tool was taking place over the surface without much deformation. Deformation was limited to the end resulting in thinning only at the end of the workpiece. On increasing rpm of the mandrel, the forces were found to increase but the deformation was not found to improve.

Table 4.11: The dimensions of the flow formed products

Sample	Initial length (l_i)	Initial thickness (t_i)	Initial Internal diameter (ID_i)	Overall Length (L_f)	Average Internal diameter (ID_f)
7075-F1 (7F01)	50	2.0	32.4	59.4	33.1
7075-F2 (7F02)	50	2.0	32.4	60.3	32.9
7075-F3 (7F03)	50	1.5	32.4	148.3	32.6
7075-F4 (7F04)	50	1.5	32.4	187	32.6
7075-F5 (7F05)	50	1.5	32.4	150.5	32.5

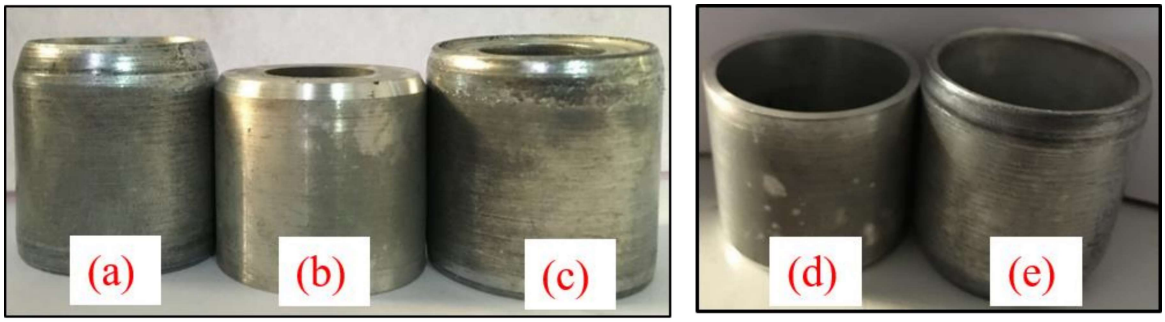

Figure 4.20 shows the flow formed samples of Al7075 7F01 that were deformed in T6 condition in presence and absence of lubrication. It is clear from the figure that under the present investigation, both the samples were hard to deform. Even with lubrication, the

maximum elongation was about 20%. This shows that there was almost negligible effect of lubrication on flow formability of small preforms with higher hardness.

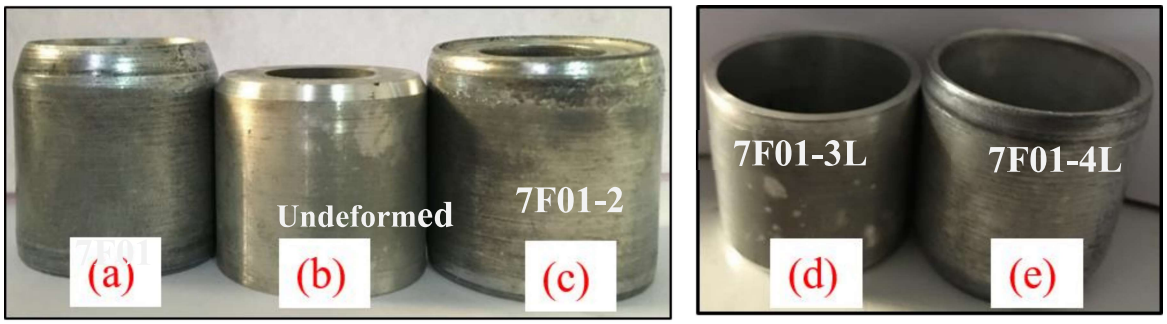

Figure 4.20: Flow formed 7F01 samples (a) 7F01 (without lubication) (b) undeformed (c) 7F01-2 without lubrication (d) 7F01-3L (with lubrication.), (e) 7F01-4L(with lubrication)

It was observed that there was slipping of the tool was taking place over the surface without much deformation. Deformation was limited to the end resulting in thinning only at the end of the workpiece. On increasing rpm of the mandrel, the forces were found to increase but the deformation was not improved significantly. During the flow forming, there were two other problems that were faced. Due to increasing forces, the torque acting on the roller became so high that the tool post holding the roller assembly started missing and it turned under the action of load. Further, as the in feed was increased, the diametral growth was found to increase making the preform loose. Two changes were done to counter the problem, Whole of the tool post was removed and the lathe dynamometer holding the roller assembly was mounted directly in place of the tool post with help of bolts. This made the mounting more rigid. Secondly, the preform thickness was reduced from 2 mm to 1.5 mm. Another trial was done with a 1.5 mm preform (7F02) with T6 temper. The flow formed part is shown in Figure 4.21. The result shows that the preform underwent an increase of 60.4 % before a crack is formed.

Figure 4.21: Flow formed 7F02 showing crack formation in the middle of the specimen.

To improve the formability of the material, annealing was done on the samples so as to reduce the strength and increase the formability. Thus the preform temper was changed from T6 to annealed condition. The annealing was done by heating by heating of samples at 470^{o}C for 3 hours and then finally furnace cooled [91]. The annealed samples were then flow formed and the result showed that the samples had much improved formability. 7F03, 7F04 and 7F05 were flow formed in annealed condition. In each cases, four passes were employed.

Figure 4.22 shows the flow formed 7F03 which cracked during the process from the middle in the third pass. The sample failed in fourth pass. The deformation was found to be the smooth in first pass. However, in the second pass the formation of wrinkles was observed which could be due to high feed and some inherent non-uniform flow. The wrinkle would be site of initiation of crack formation in the successive passes. The high magnitude of radial load exerted by the roller may have caused the failure. Figure 4.22 also shows the other defects present such as wrinkles and presence of serrated region. The SEM fractogaphs of the fractured portion has been discussed in section 4.2.5.6.

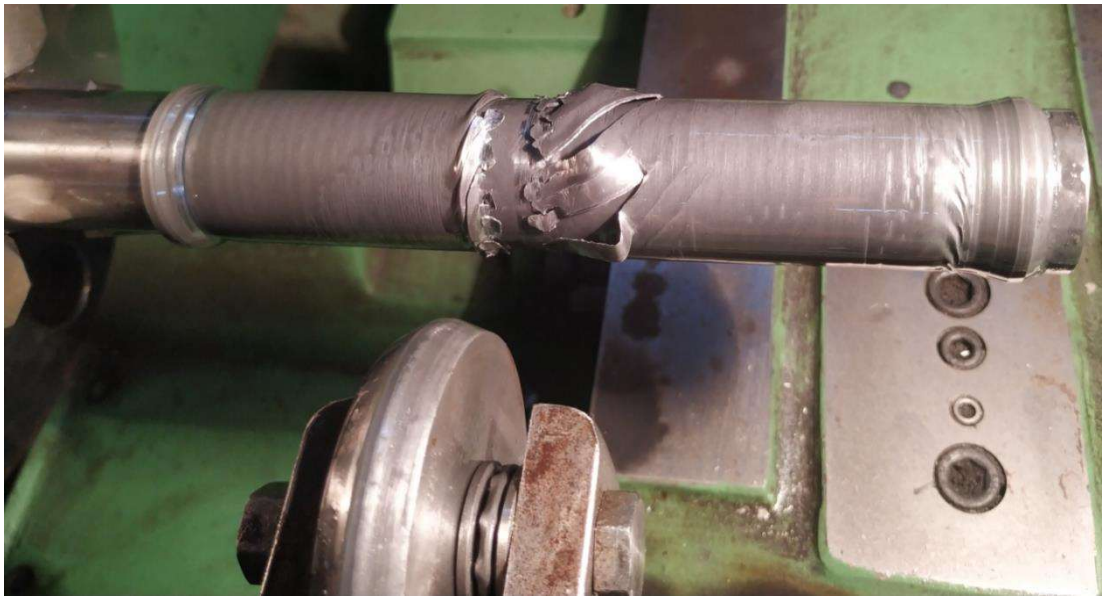

(a)

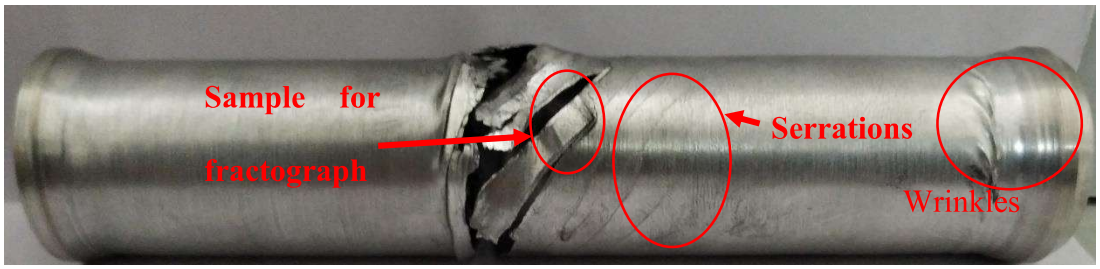

(b)

Figure 4.22: Flow formed 7F03 (a) Experimental view (b) defects present

The flow forming 7F04 showed uniform elongation and didn't fail during the investigation. The length was limited by the length of the mandrel available for deformation

Table 4.12 shows the dimensions of undeformed preform and flow formed 7F04. Figure 4.23 shows the flow formed product 7F04.

Table 4.12: Summary of geometrical characteristics of the preform(undeformed) and deformed 7F04

Dimensions	Preform dimension	Product dimension
Inner dia (mm)	32.4	32.4 (throughout), 32.5 (near ends)
Thickness (mm)	1.5	0.5
Length(mm)	55	187

Figure 4.23 Flow formed Al7075 annealed sample 7F04

. The surface roughness measured in 7F04 was having Ra of 0.425μm , excluding some portion at start and end where roller marks and some amount of wrinkling was present. Figure shows the flow formed sample 7F05 which was flow formed in 4 steps.

Figure 4.24: Flow formed 7F05

7F05 was formed with constant feed but the start point of the roller was shifted to produce stepped product. The product failed in third step as shown in Figure 4.24. The fractograph of the fractured sample is shown in section 4.2.5.6.

4.2.2 **Force Measurement**

The in-situ force measured, by lathe dynamometer, in different passes of 7F04 are given in Figure 4.25.

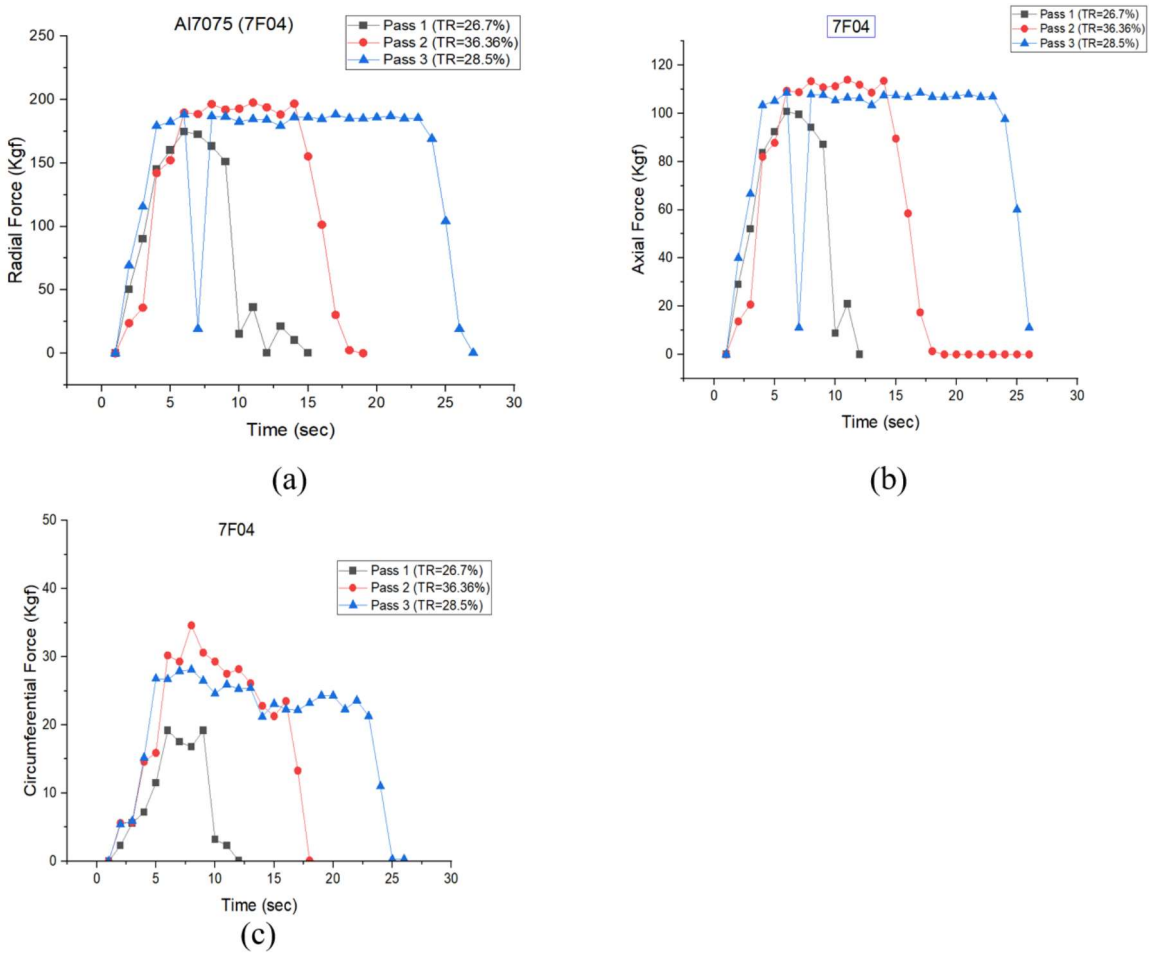

Figure 4.25: Flow forming forces in Al7075 –O (7F04) (a) radial force (b) axial force (c) circumferential force

4.2.3 **XRD analysis**

Figure 4.26 shows the X-ray diffraction pattern of the Al7075 T6 specimen. Analysis of peak depicts the presence of α-Al solid solution phases (PDF#85-1327) along with GP Zone (MgZn2)(PDF#65-3578), η' and η (PDF# 77-1177), $CuAl_2$ intermetallic compounds (PDF#89-1980) in the 7075-T6 heat treated aluminum alloy. Intensity of the transition precipitates (GP-Zones, η' and η) reduces while giving 20% and 40% deformation to the as received 7075-T6 aluminum alloy. The average crystallite size (D) and lattice microstrain (ε) values dislocation density was given in the Table 5.1. XRD pattern for 7F02 is shown in Figure 4.27.

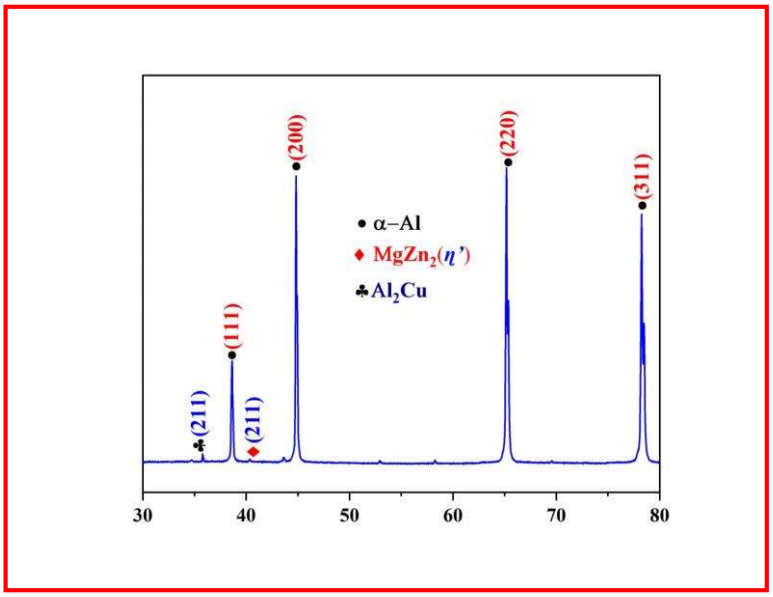

Figure 4.26: X-ray diffraction pattern of the Al7075-T6 Aluminum alloy

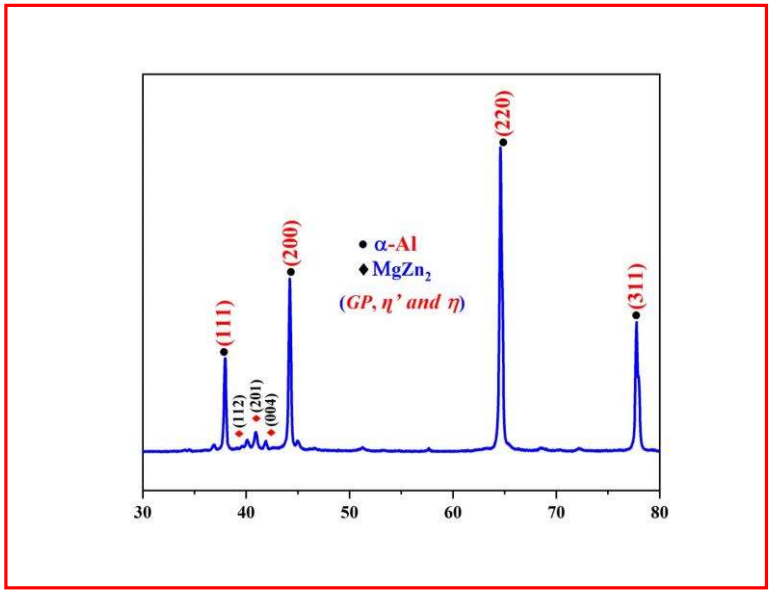

Figure 4.27: X-ray diffraction pattern of the 7F02 Aluminum alloy

Absence of the $Al_2Cu(\theta)$ phases into the Figure 4.27 in the cold deformed 7075 aluminum alloy indicates dissolution of the phases. Heat generation as well as formation of the dislocation structures is generally noticed during the cold deformation. Former is related to the internal friction between the atoms inside the materials. Whereas, latter is pertaining to the induced strain field inside the materials. Therefore, thermally induced and dislocation

shear assisted dissolution may be the possible cause. However, the amount of heat released during the flow forming process was found to be around 60°C which is not sufficient for thermally induced dissolution of the phases. Hence we can consider that the dislocation shear induced dissolution may be the cause of the dissolution mechanisms.

4.2.4 EBSD Analysis

The EBSD analysis of the Al7075 T6, Al7075- O annealed and flow formed 7F03 and 7F04 are presented in this section. Figure 4.28 shows the inverse pole figure of Al7075 T6 samples shows that the most of the crystal are oriented in (111) direction.

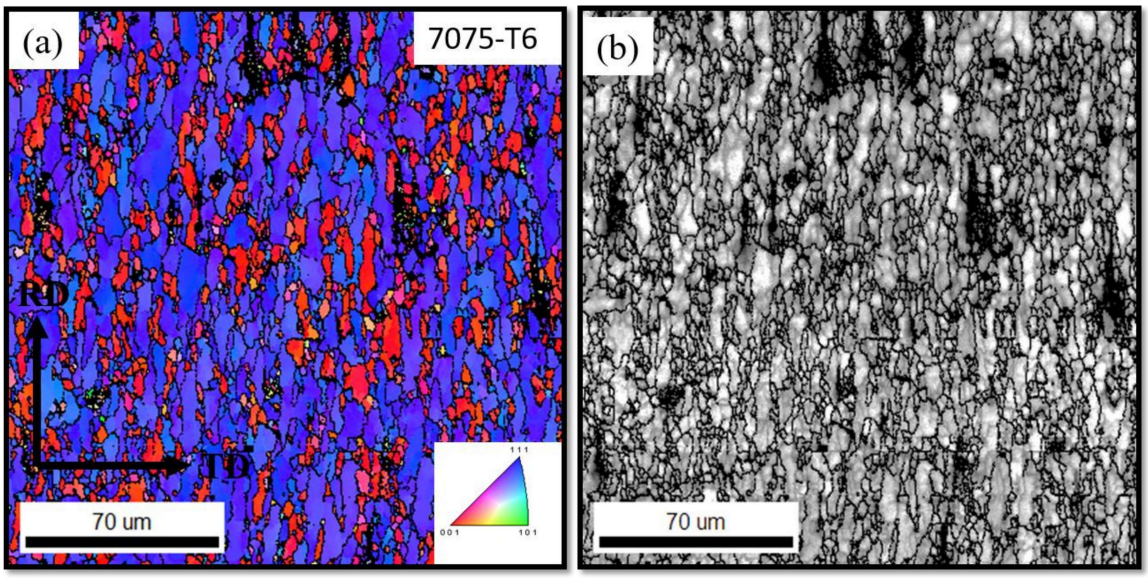

Figure 4.28: EBSD result of flow formed Al7075 T6 (a) Inverse pole figure map (b) Image quality map

Figure 4.29 shows that the fine grain size present in the as received sample 7075 T6 sample. Grain size of 9.15314 $\boldsymbol{\mu m}$ was found to have the highest area fraction.

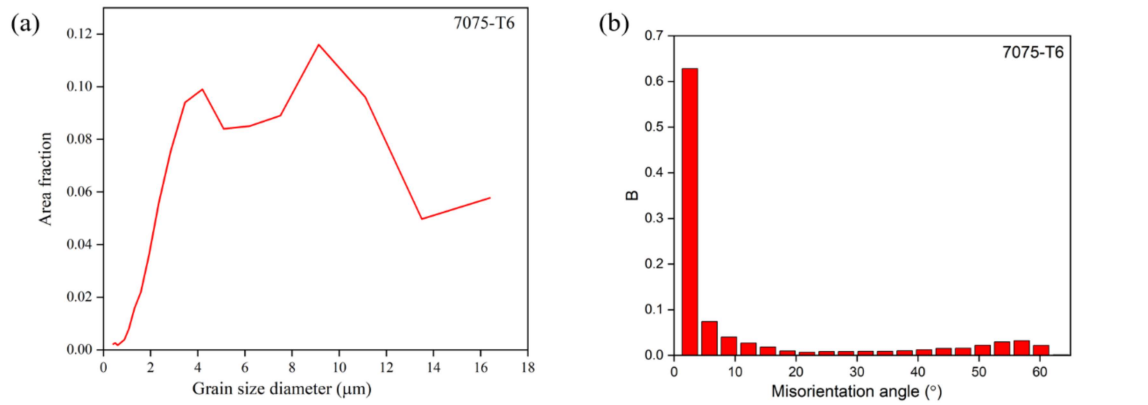

Figure 4.29: (a) Grain size distribution in annealed undeformed Al7075 sample (7075-T6) (b) Misorientation angle distribution in 7075-T6

Misorientation angle analysis (Figure 4.29) in as received sample shows high proportion of Low angle grain boundaries which is responsible for its high hardness. To compare the effect of annealing treatment on grain size, the EBSD analysis was done on one of the annealed undeformed samples. Figure 4.30 shows that the orientation image map of Al7075-O.

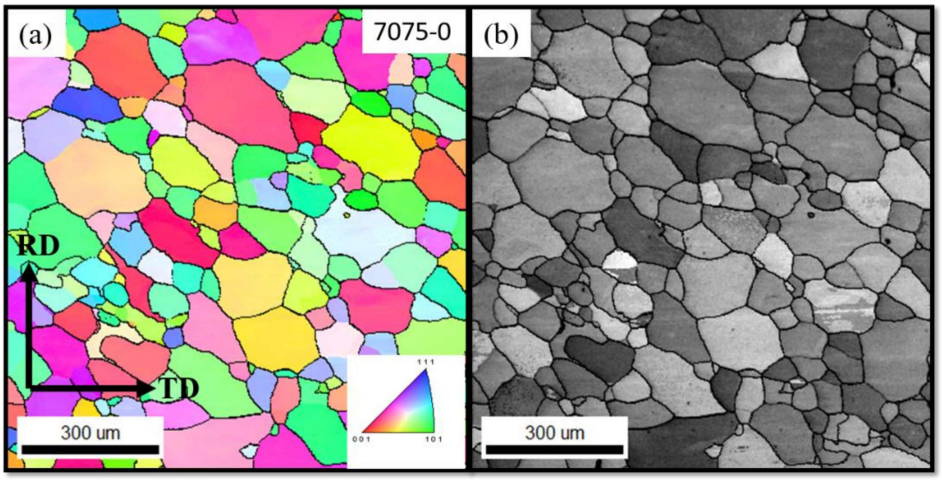

Figure 4.30: EBSD result of annealed Al7075 preform (a) Inverse pole figure map (b) Image quality map

The OIM shows that the presence of large grain size as compared to as received samples which has maximum fine grain structure. Figure 4.31 shows that average grain size diameter of 147.12 μm has maximum area fraction. This was almost 16 times larger than those present in as received samples. Crystals are found to be randomly orientated in annealed samples as compared to as received samples.

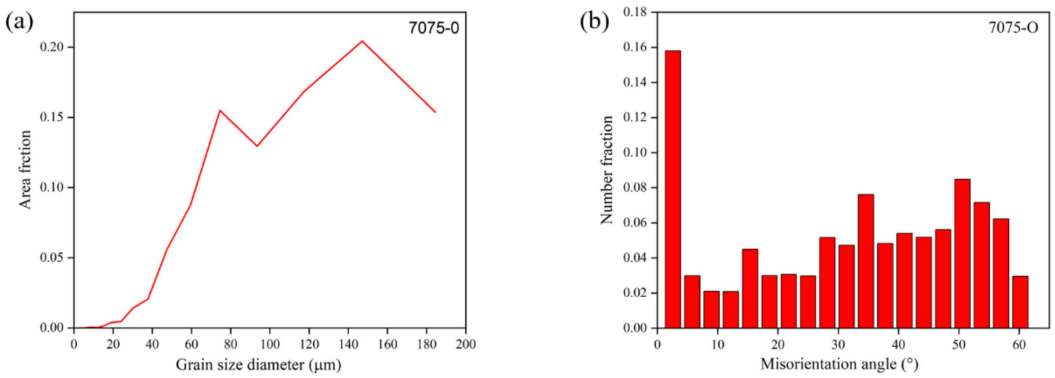

Figure 4.31: (a) Grain size distribution in annealed undeformed Al7075 sample (7075-O) (b) Misorientation angle distribution in 7075-O

Comparing the Misorientation angle, it was found that both the low angle and high angle grain boundaries are present in annealed preform but high angle grain boundaries are very less in as received sample.

The effect of flow forming of grain size and crystal orientation with respect to the annealed undeformed preform can be compared by comparing the orientation image, grain distribution and misorientation angle data.

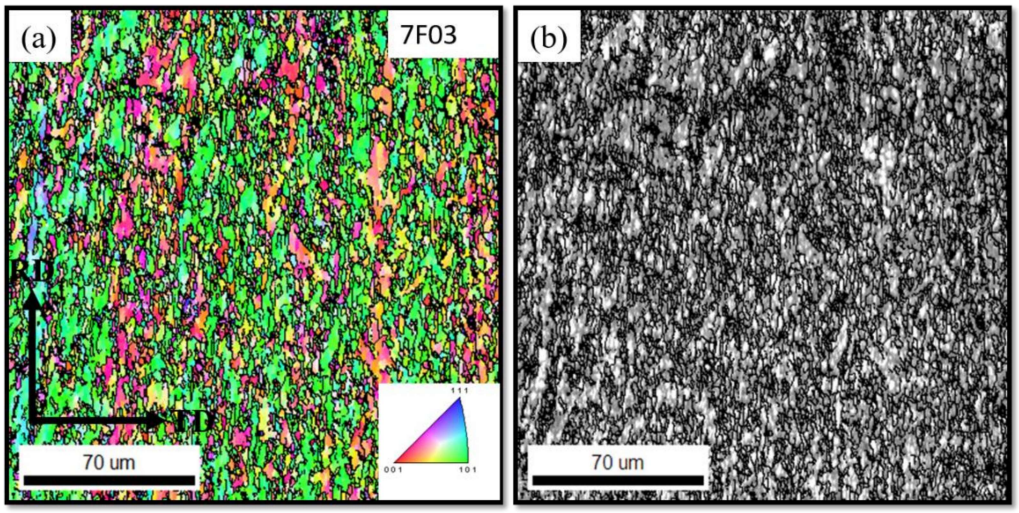

Figure 4.32: EBSD result of flow formed 7F03 (a) Inverse pole figure map (b) Image quality map

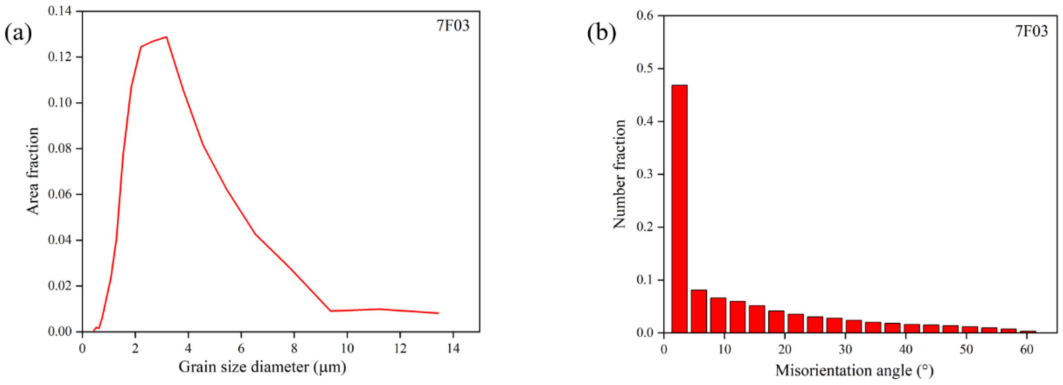

Figure 4.33: (a) Grain Size distribution in sample 7F03 (b) Misorientation angle distribution

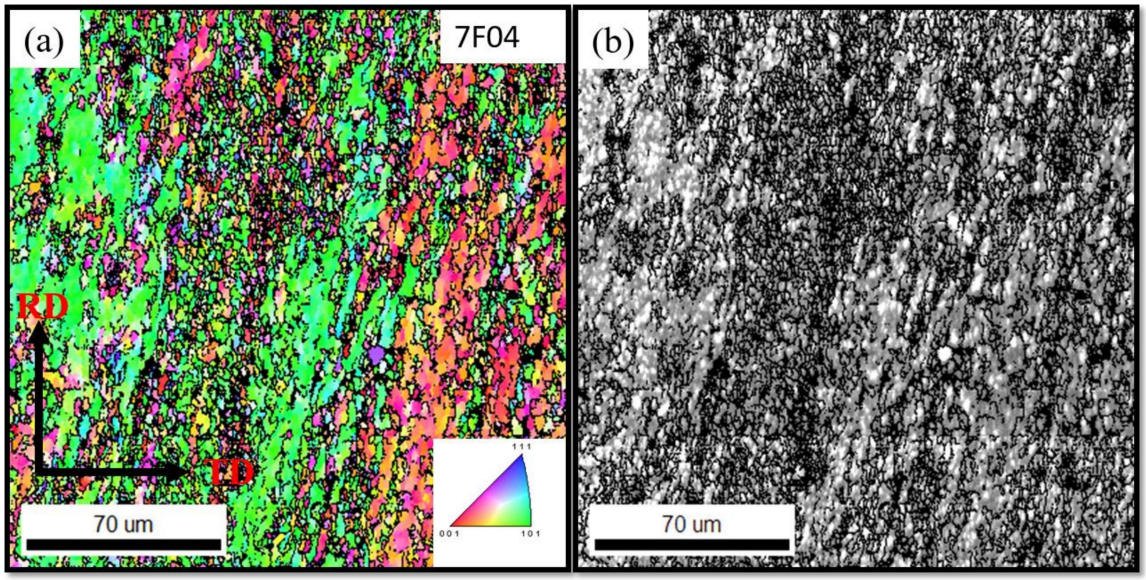

Figure 4.34: EBSD result of flow formed 7F04 (a) Inverse pole figure map (b) Image quality map

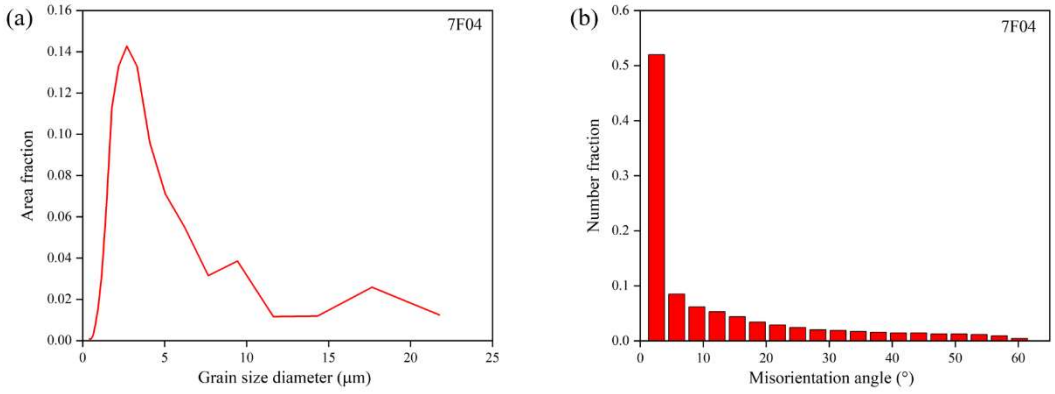

Figure 4.35: (a) Grain Size distribution in sample 7F04 (b) Misorientation angle distribution

4.2.5 **Defects in Flow forming**

The defects that were encountered while performing the flow forming of different samples of Al7075 are discussed in this section. The defects that were mainly formed were flange

formation at end, chip formation, circular marls on roller surface, distortion of job, diametral growth and the crack formation.

4.2.5.1 Defect 1: Flange formation at the end (backward flow)

Figure 4.36: Backward flow defect leading to flange formation

The problem of flange formation was common while working Al2014 T6 and Al7075 T6 samples. The average flange length in Al7075 T6 was found to be around 2 mm. The flange length was found to increase when in-feed was increased. The problem was found to be more when chamfer was either not present or both chamfer length and chamfer angle was too small. In the present investigation, a chamfer angle of 30 degree and chamfer length of 5mm greatly reduced the problem in Al6101 T6 samples and in annealed samples of A7075 and Al2014.

4.2.5.2 Defect 2: Chip formation

Chip formation is one problem that was encountered when the roller is not free to rotate about its axial movement. Small chips has been found in sample trials done on Al6063 preform and also in flow forming of Al7075in as received condition. (Figure 4.37)

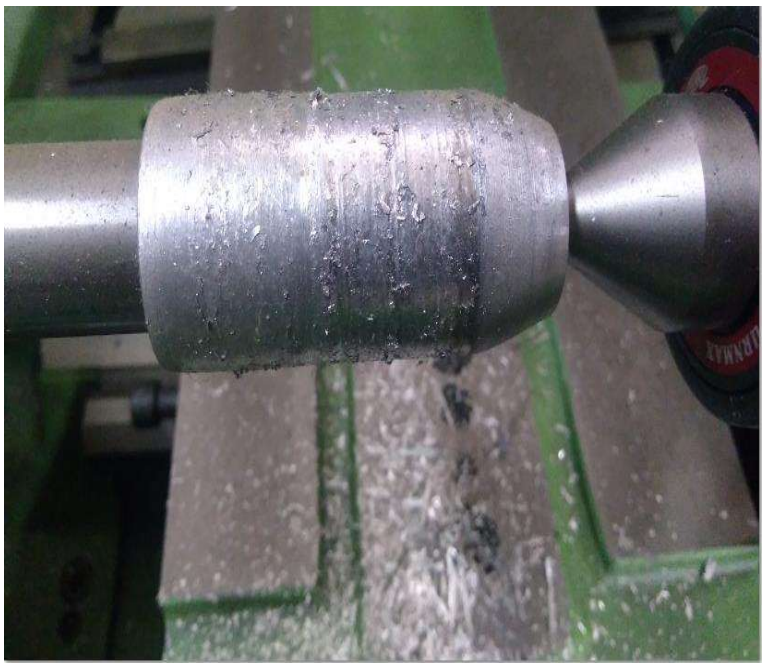

Figure 4.37: Defect: Chip formation during flow formation.

The problem of chip formation has been found to be more when the thickness of preform increases, resulting in higher force. The problem has been found in 7F01 samples when mandrel speed was 420 rpm or more and in feed was higher. However, this problem has not been observed after roller assembly was modified and bearings were introduced.

4.2.5.3 Defect 3: Circular marks on roller

The problem of circular marks on the surface would tend to `arise when there would be physical conatct between the Y frame and roller surface. The interaction would occur when the roller deflects under the action of axial force.

Figure 4.38: Defect: Circular marks in Roller

The problem was removed when the roller assembly was modified and a thrust bearing was introduced.

4.2.5.4 Defect 4: Distortion of job

Distortion of job was seen in initial trials of flow forming on Al6063 samples near the fixed end of the preform. Figure 4.39 shows the problem of bending of job. Bending of job occurs when the mandrel deflects under the action of radial force either due to lack of firm support or due to buckling of the mandrel under the action of load.

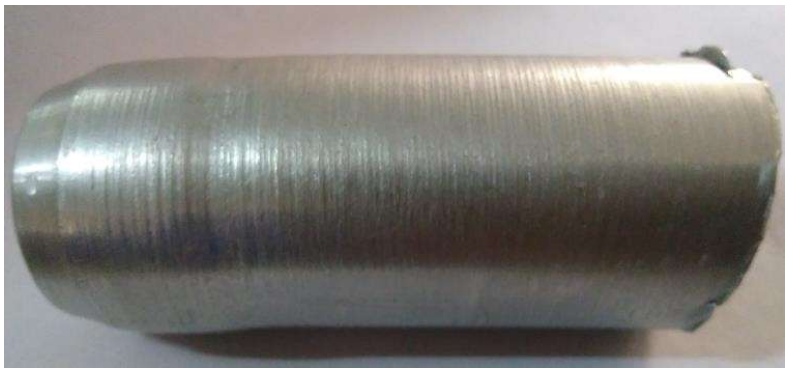

Figure 4.39: Bending of Job Flow formed Aluminium 6061(as received) with Roller attack angle of 30°. Rotation speed of 420 RPM.

4.2.5.5 Defect 5: Diametral growth

Diametral growth was found in almost all samples. In the present investigation, diametral growth was highest in flow forming harder samples such as 7F01, 7F02. Diametral growth in FF01 and FF02 led to the failure of the flow forming as once the diameter of the sample increases, the preform starts rotating over the mandrel. Table 4.11 shows the preform (undeformed dimensions) and deformed dimensions.

4.2.5.6 Defect 6: Formation of Crack

In the present investigation, flowforming was done till the workpiece failed. 7F01 and 7F02 failed as only thinning at the end was taking place and slipping of roller over the surface. However, most of the samples failed due to crack formation. Figure 4.40 shows of the cracked samples.

(a) (b) (c)

Figure 4.40: Defect: Crack formation in flow formed samples (a) 7F02 (b) 7F03 and (c) 7F05

The failed regions of the cracked samples have been analysed by SEM. The fractograph of fractured portion of 7F02 has been shown in Figure 4.41. SEM analysis of the fractured portion was done. The SEM was done on bench top SEM present at CIF, IIT (BHU)

Varanasi. The results of the same are presented in Figure 4.41. The fractograph shows secondary particles which would have formed due to decohesion. These secondary particles would have resulted in crack formations.

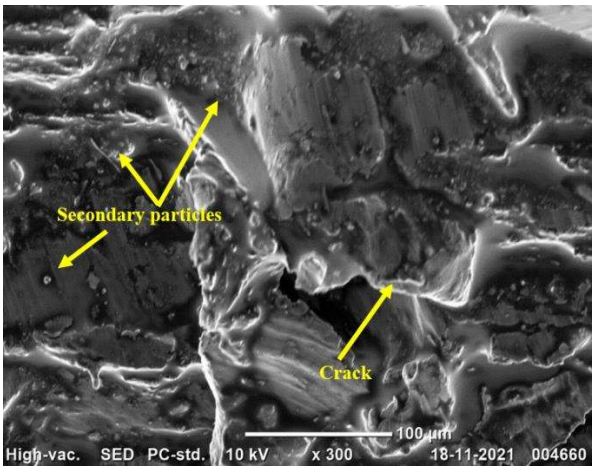

Figure 4.41: Fractograph of 7F02

The fractograph of 7F03 is shown in Figure 4.42. The sample was taken from the fracture region from the encircled portion. The fractured section showed a delamination region.

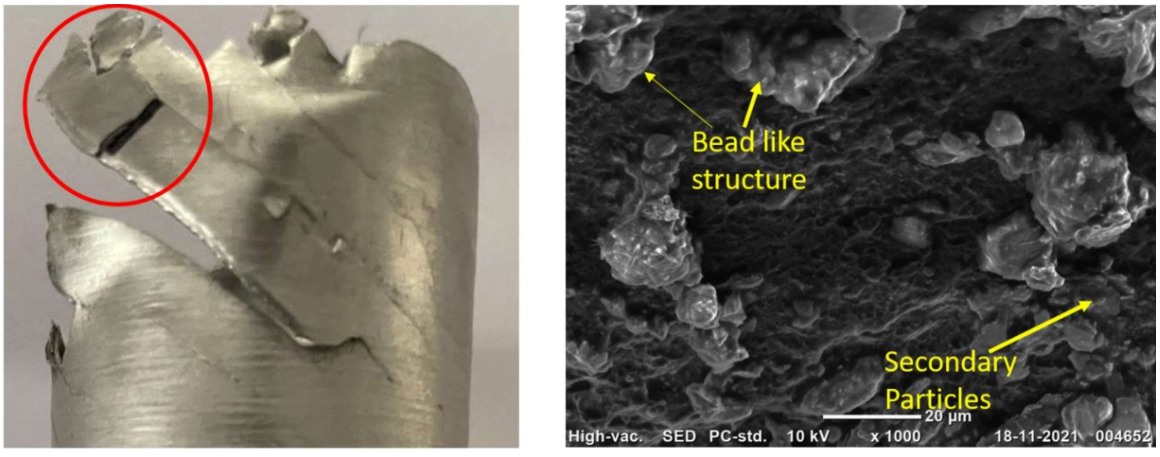

(a) (b)

Figure 4.42: (a) Fractured portion of 7F03. Sample for fractograph has been taken from encircled region. (b) SEM fractograph of 7F03

This failure was observed when the roller applies radial load over a wrinkled region of previous pass. The presence of large bead shaped morphology suggests the morphology similar to weld bead. This would probably formed due to formation of semi-solid or viscous zone due to localised melting under the combined action of high load and friction. Secondary phase particles are also seen.

Figure 4.43 shows the defects in flow formed sample 7F05. The material failed with crushed section in the middle. The end section also shows cracked portion starting from the flange portion that also represents the region from where the roller has been removed.

Figure 4.43: Flow formed 7F05 (a) preform and flow formed product (b) crack near the end and ovality at end section.

The failure of 7F05 was found to occur in the third pass. The fractograph of the fractured sample taken from cracked region of 7F05 is shown in Figure 4.44.

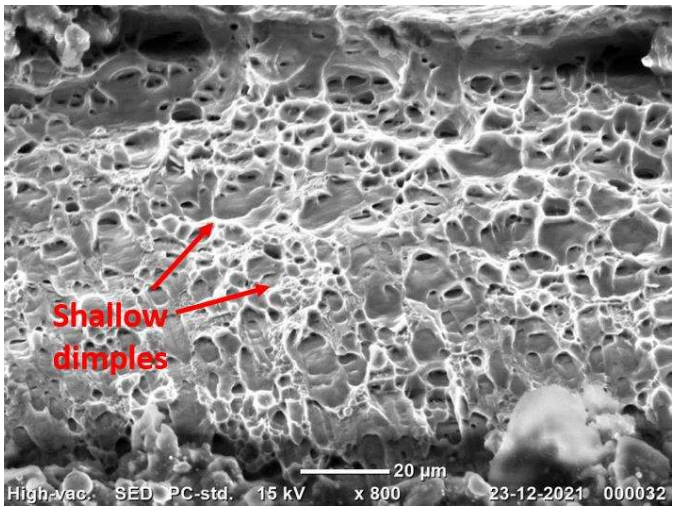

Figure 4.44: Fractograph of a cracked portion of 7F05

Presence of large number of dimples shows that the the material has fractured in ductile mode. However, the dimples are found to be shallow, showing that dutility of the sample was lower. The lower ductility also predicts that grain refinement during flow forming process.

4.2.6 **Microhardness**

Vickers hardness test was done on the flow formed Al7075 samples. The results are shown in Figure 4.45. The hardness of as-received samples was found to be 175 HV. The hardness of the preform samples after annealing treatment was found to be 69.3 HV. After the flow forming operation, the hardness was found to increase to 94.92 HV in 7F04 after the final pass. The hardness was thus increased by about 37% after the flow forming operation. Similar increase in hardness was found in 7F03 and 7F05.

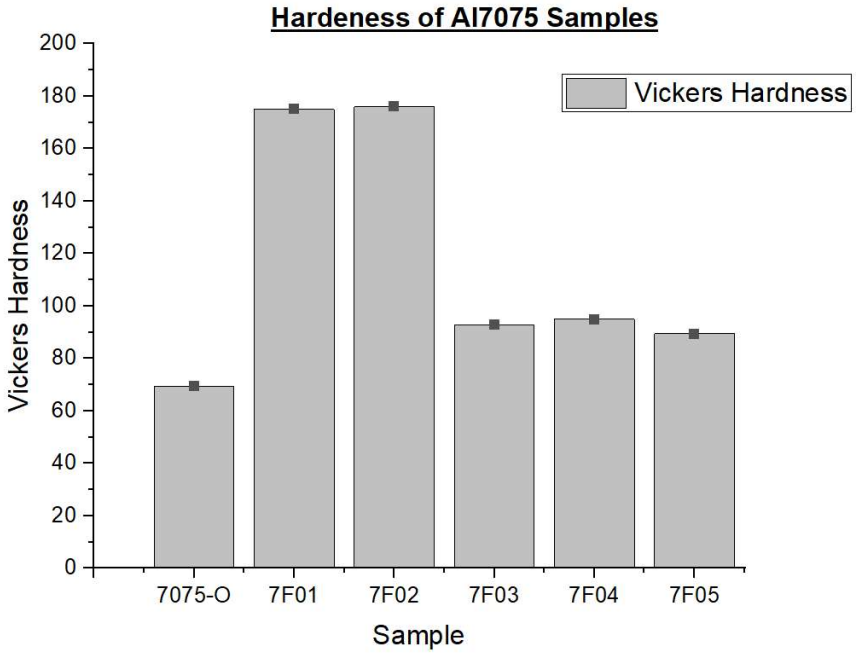

Figure 4.45: Hardness of undeformed and flow formed samples

4.3 EXPERIMENTAL RESULTS OF FLOW FORMED AL2014 SAMPLES

4.3.1 Introduction

The samples were prepared from the rod supplied by M/s All India Metal Corporation. The rods were machined to the required dimensions. Then the inner diameter was maintained by boring using a single point boring tool. . The samples were prepared and the force measurement was done during the experiment using a lathe dynamometer. The samples were then heat treated at 413 °C for 2 hours and then furnace cooled. The deformation was carried out at the process parameters used in Al7075 to observe the behaviour of Al2014 preform on parameters similar to that used in experimentation

4.3.2 Material Specification:

The chemical composition of the preform was found to be in Table 4.13

Table 4.13: Chemical Composition of Al2014

Al	Si	Cu	Mn	Mg	Zn	Fe	Ti+Zr	Cr
Rest	0.8	4.4	0.6	0.5	0.2max	0.5	<0.15	0.08

The experimentation was conducted on five samples. The samples were named 2014-01, 20214-02, 2014-03, 2014-04, and 2014-05. In the case of the 2014 -01 preform, the workpiece failed during deforming in the T6 temper condition. The SEM image of the fractured surface was then analyzed. The tensile specimen was prepared and unidirectional tensile testing was done at IIT Kanpur.

Figure 4.46 shows the flow formed specimens. The specimens 2014-01, 2014-02 and 2014-03 were of T6 temper while 2014-04 and 2014-05 were first annealed at by heating the samples at 413°C for 2 hours.

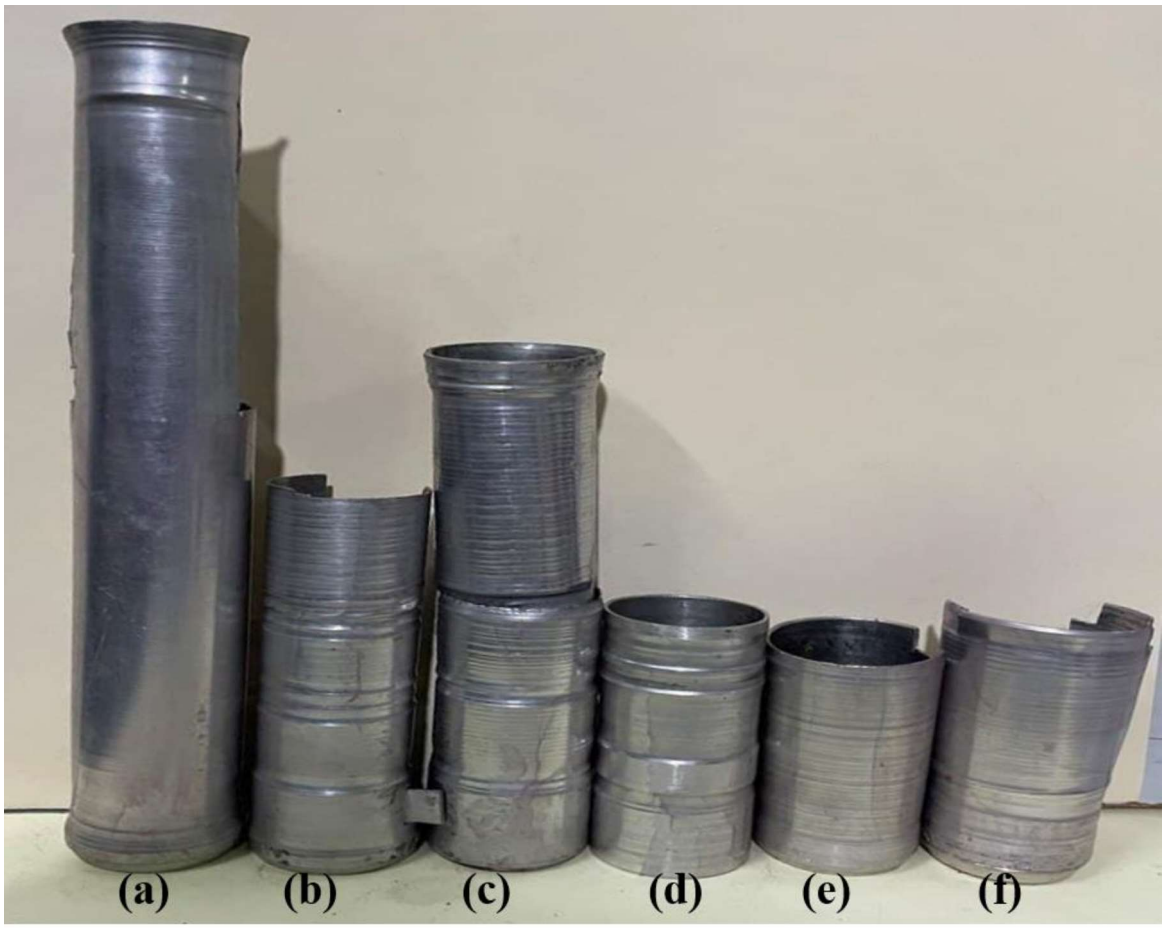

Figure 4.46: Flow formed Al2014 Samples (a) 2014-05 (b) 2014-04 (lower) (c) 2014-03 (d) 2014-04 (upper) (e) 2014-02 (f) 2014-01

The preform dimensions are given in Figure 2.2. After the machining, the preform were softened by heating the preform at 413ºC for 2 hours and furnace cooling. The preform were then deformed at two different RPM of 240RPM and 420 RPM at different thickness reduction and at two different feed rates of 0.04 and 0.08mm/min

4.3.3 **Flow forming forces**

In situ force measurement was done using a lathe dynamometer. The forces are plotted against time steps as shown in Figure 4.47 and Figure 4.48

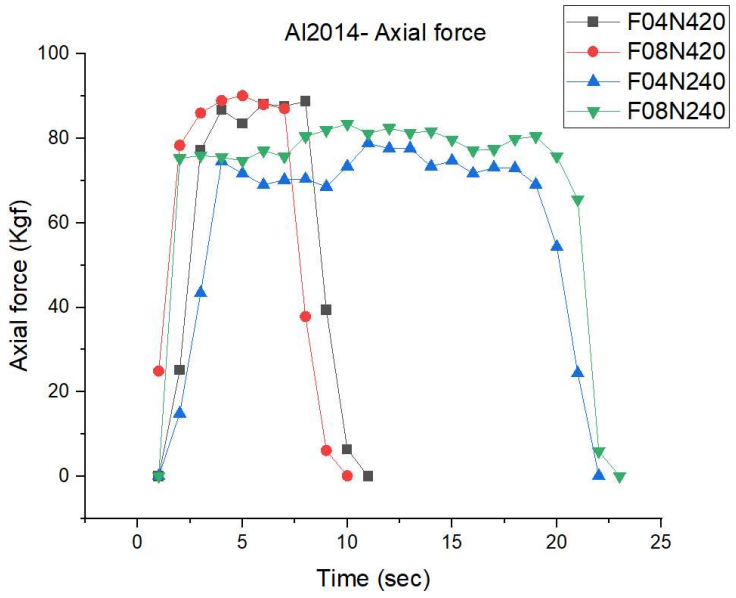

Figure 4.47: Axial force variation during flow formation of Al2014

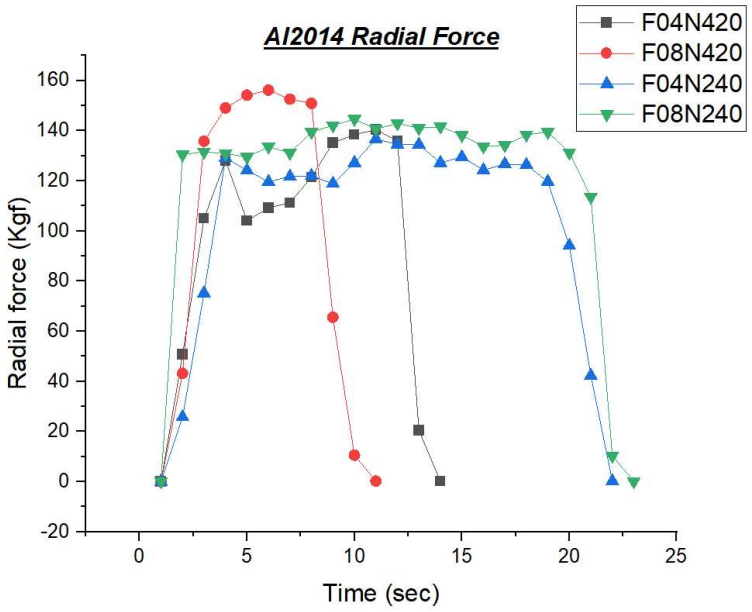

Figure 4.48: Radial Force variation in Al2014 flow formed sample.

The sample F04N240 has been deformed at a feed rate of 0.04mm/min and mandrel rpm of 240 rpm. Similarly, sample F08N240 has been deformed at 0.8mm/mm feed and mandrel rpm of 240.

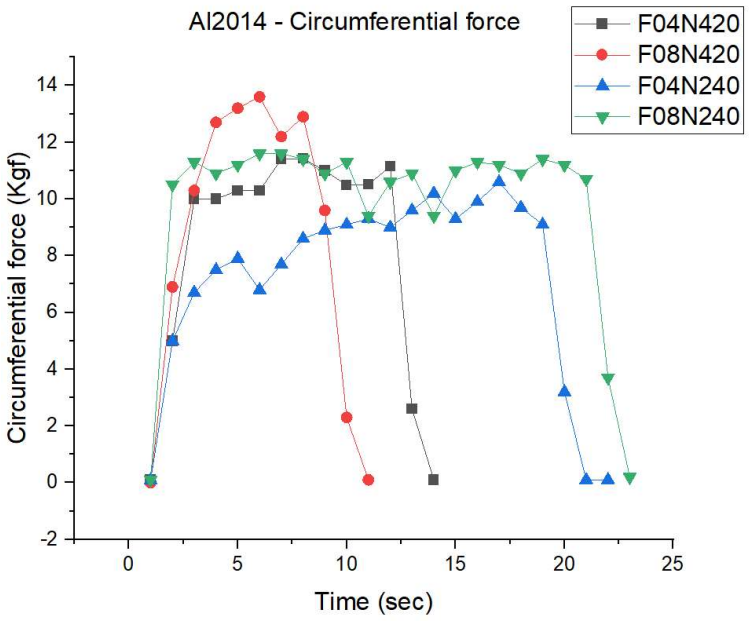

Figure 4.49: Circumferential Force variation in Al2014 flow formed sample.

The force measurement shows that the radial force dominates and the circumferential force was found to be the least.

It can be seen from the table that in the present investigation, all the three components of forces were found to increase with increasing thickness reduction. The forces were found to be higher in T6 temper of the preform as compared to heat treated condition. The radial force was found to higher among all components of the forces.

Diametral growth in Al2014 flow formed samples Al2014-03 and 04 are shown in Figure 4.50. As clearly seen from the table the problem of diametral growth is more pronounced near the end of the flow formed tube. It can be seen that the figure that the diametral growth near the fixed end was around 0.1 mm but it was found to increase to 0.3 mm around the exit of the tube where the tube diameter increased to 32.7mm.

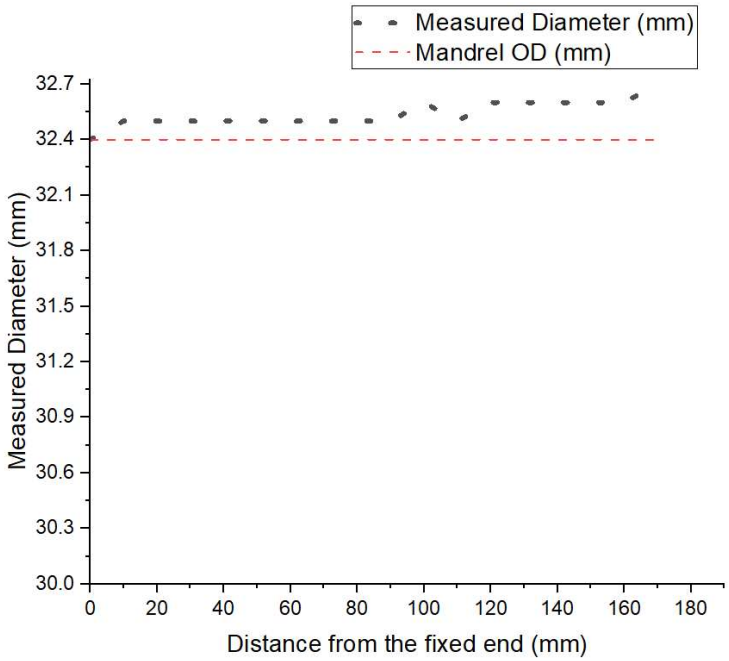

Figure 4.50: Diametral growth along the fixed end of the workpiece

The tensile test of the Al2014-03 was done and compared with the heat treated preform sample. The results showed that the tensile strength increased from 252.10 MPa in heat treated preform to 276.57 MPa in flow formed sample. This could be due to increase in dislocation density. [92][93]

4.3.4 **Microhardness Test**

Figure 4.51 shows the result of hardness on undeformed Al2014 samples (Al2014-O) and flow formed samples 2014-01 to 2014-05 samples. The results show that the hardness increases from 42 HV in undeformed heat treated Al2014 samples to 87.2 HV in flow formed 2014-5. The two samples 2014-1 and 2014-2 showed high hardness as these samples are flow formed in T6 condition. The initial preform hardness of Al2014 was 130 HV.

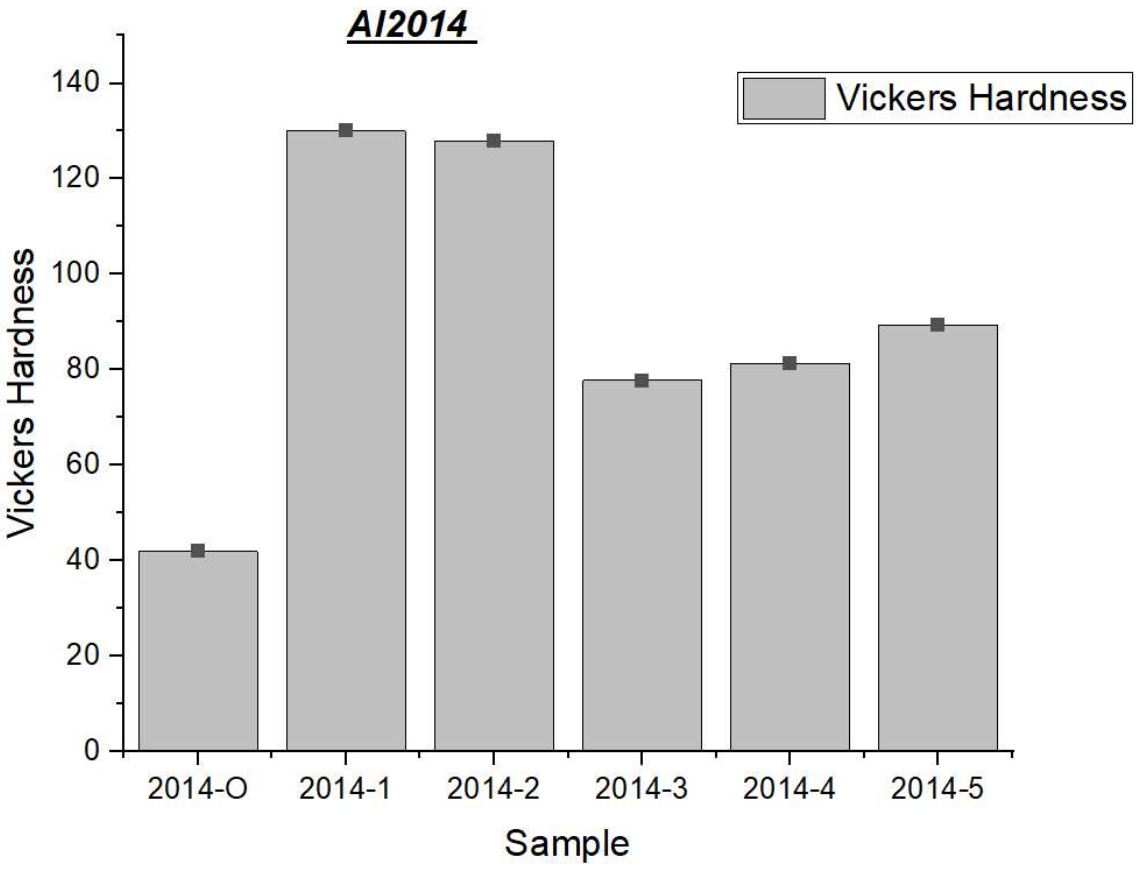

Figure 4.51: Hardness variation of preformed and flow formed samples

4.3.5 **XRD Analysis**

XRD analysis was done X-ray diffraction Pattern of Al2014 undeformed and flow formed samples. Figure 4.52 shows the X-ray diffraction pattern of the undeformed annealed sample. The XRD pattern shows higher intensity of $\alpha - Al$ along (200), (220) and (311) planes. Small intensity of Al_2Cu (θ and θ') were visible in plane (112) and (310).

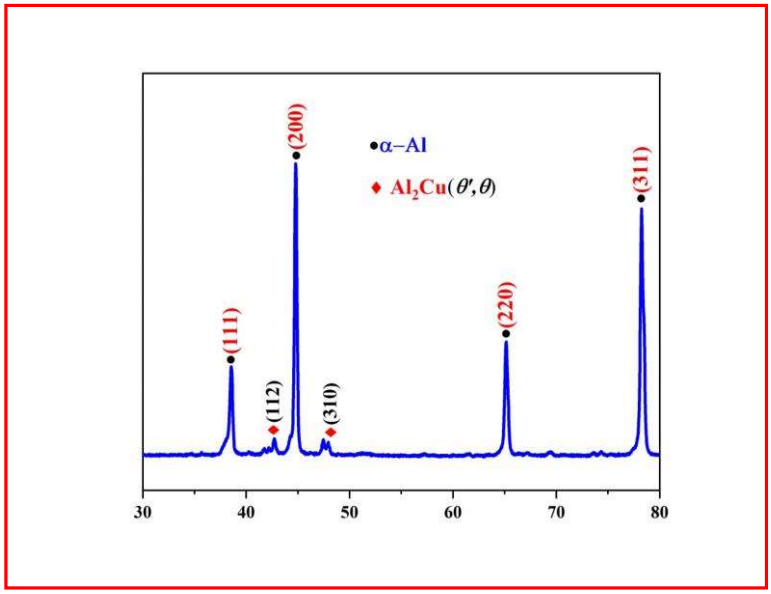

Figure 4.52: X-ray diffraction pattern of the as annealed Al2014 preform

The X- ray diffraction of the flow formed is shown in Figure 4.53. The diffraction pattern shows that the intensity of $\alpha - Al$ decreases on plane (311) and (220).

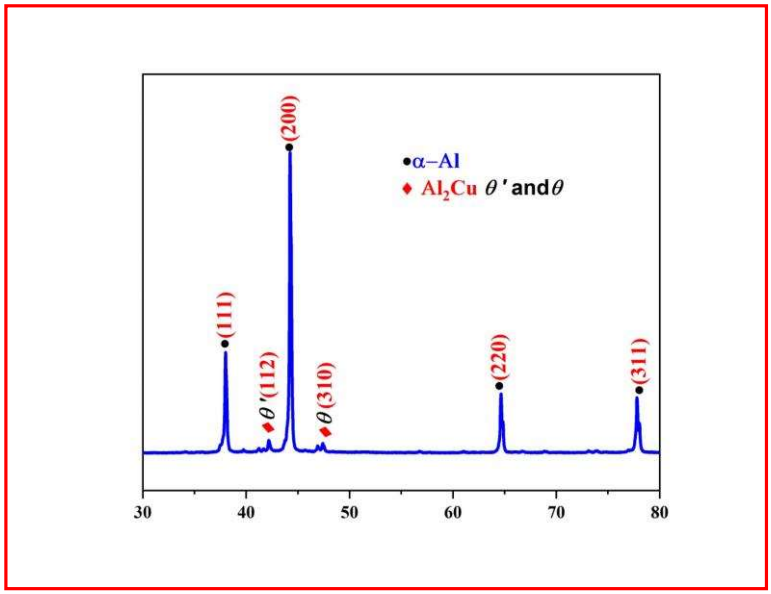

Figure 4.53: X-ray diffraction pattern of the flow formed 2014 Aluminum alloy 2014-05

The crystallite size, lattice microstrain, and dislocation density were also calculated based on intensity peaks. The crystallite size was found to decrease from 11.7 Å in annealed preform to 6.50 Å in flow formed sample. However, lattice microstrain was found to increase from 12.71% in the annealed sample to 15.38% in flow formed sample. Similarly, the dislocation density was also found to increase from 37 X10^{17}/m^2 to 73 X 10^{17}/m^2.

4.3.6 EBSD Analysis

The EBSD analysis of 2014 samples were done in as received T6 temper, annealed and flow formed condition. Figure 4.54 gives the inverse pole figures for annealed Al2014 sample. The figure shows most of the grains are oriented along (101) axis.

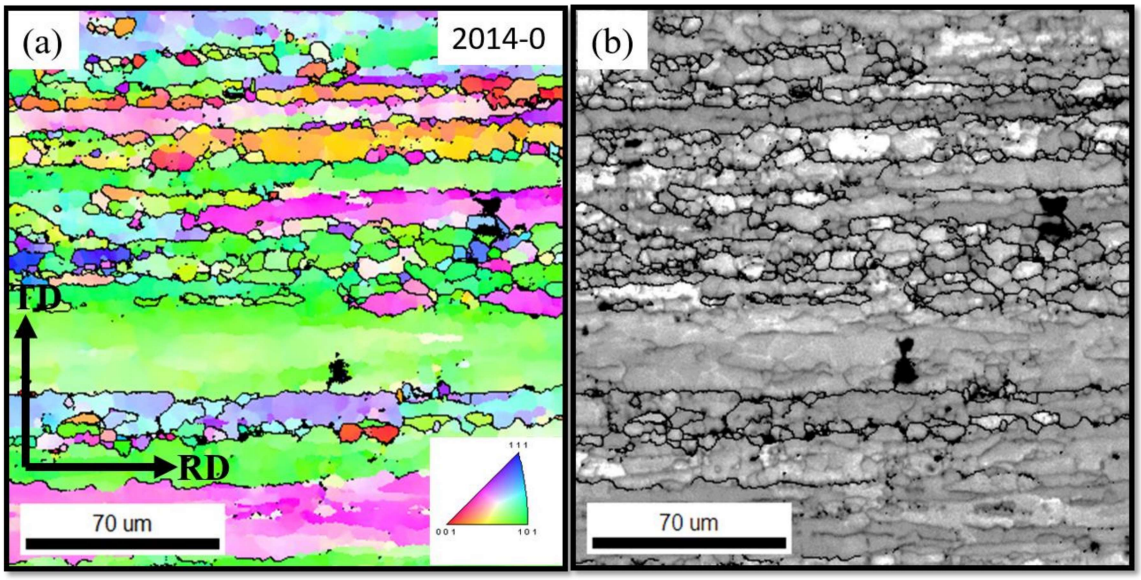

Figure 4.54: EBSD inverse pole figure map of undeformed 2014-O annealed sample (a) Inverse pole figure map (b) Image quality map

Presence of large size grains in annealed samples is indicated by the inverse pole figure. Grain distribution graph (Figure 4.55) showed presence of large size grains in the annealed sample. Average grain size of 90.2 μm was found to occupy maximum area fraction.

Analysis of misorientation angle Figure 4.55 showed that the low angle grain boundaries were dominant in the sample analyzed.

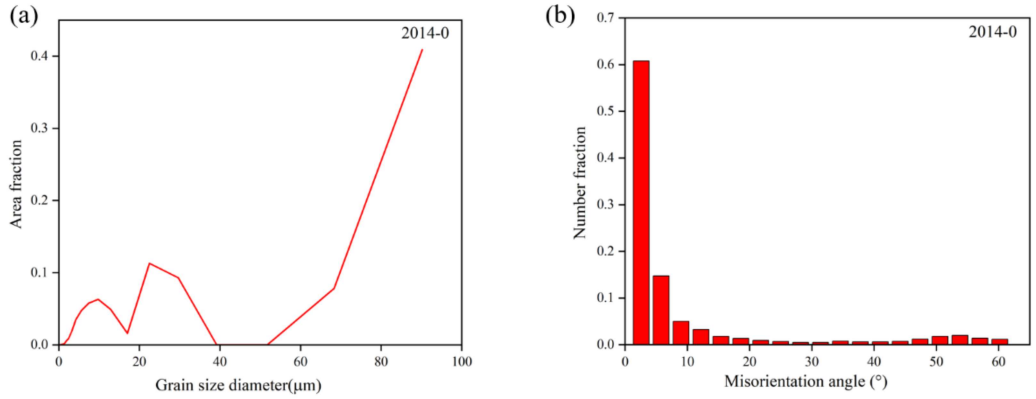

Figure 4.55: (a) Grain size distribution in 2014-O (b) Misorientation angle in 2014-heat treated at 413ºC for 2 hour.

Figure 4.56 shows the inverse pole figure for Al2014 T6 as supplied sample. The inverse pole figure showed crystals heavily oriented towards <111> direction. Relative smaller sized grains (from Figure 4.57) were present in the sample. Average grains size of 46.4276 was found to occupy the largest area fraction.

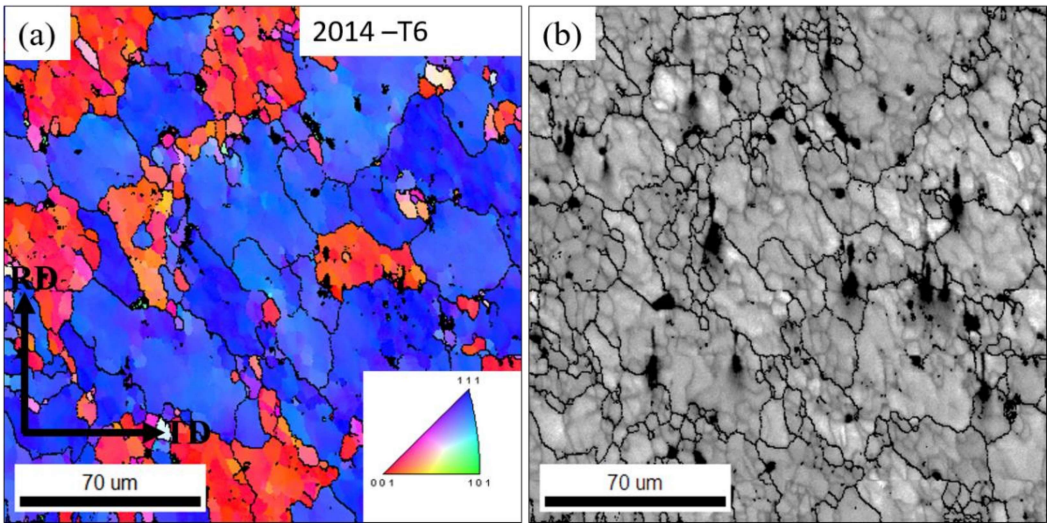

Figure 4.56: EBSD result: inverse pole figure for flow formed 2014-T6 sample (a) Inverse pole figure map (b) Image quality map (c) (001) inverse pole figure

As compared to annealed samples, low angle grain boundary was dominating in as received angle. Comparatively, the misorientation angle of 2.6° occupied almost 80 pecent number fraction in as received samples while number fraction of misorienation angle of 2.6° in annelaed sample was 0.608.

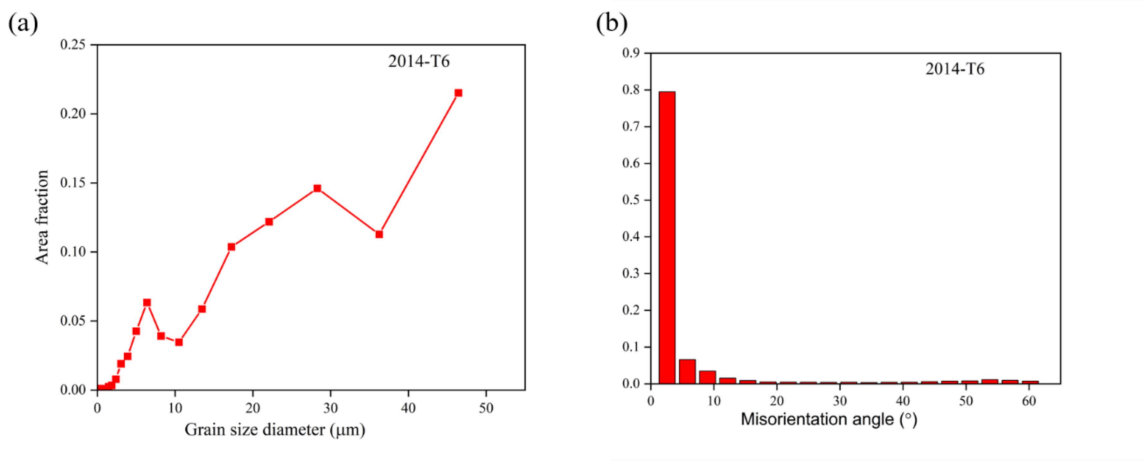

Figure 4.57: (a) Grain Size distribution in 2014-T6 (b) Misorientation angle in 2014-T6

The inverse pole figure for flow formed samples 2014-2 is shown in Figure 4.58. Grain size distribution and misorientation angle data are given in Figure 4.59. Large sized grain of average diameter of 80.75 μm and 61.27 μm are found to have highest area fraction. The sample also contained low angle grain boundaries with misorientation angle of 2.6° occupied almost 0.7 number fraction.

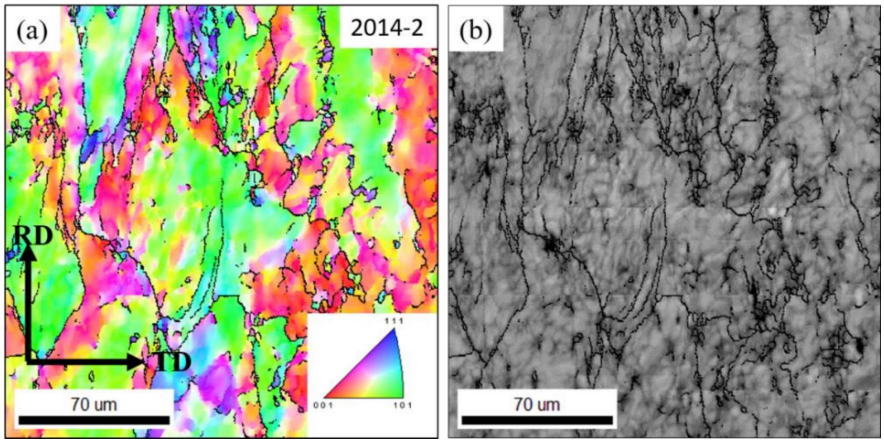

Figure 4.58: EBSD result of flow formed 2014-2 sample (a) Inverse pole figure map (b) Image quality map (c) (001) inverse pole figure

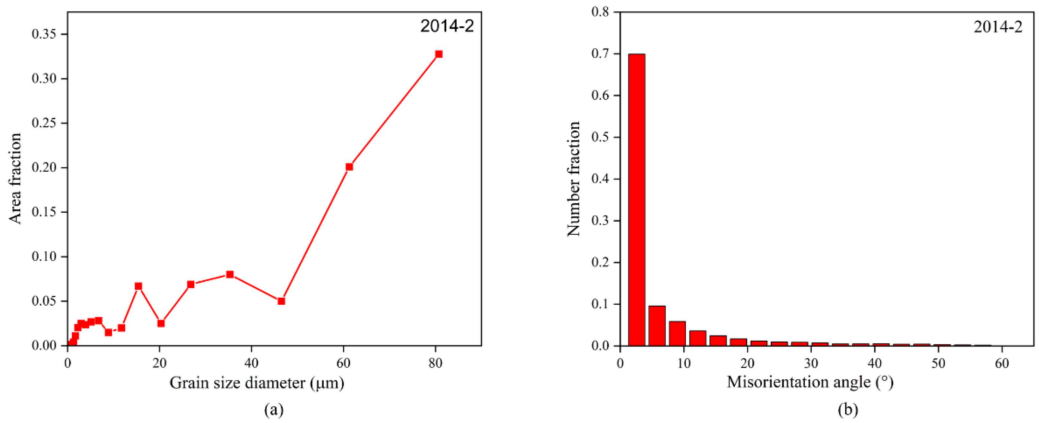

Figure 4.59: (a) Grain Size distribution in 2014-2 (b) Misorientation angle in 2014-2

4.3.7 **Defects encountered in Al2014 samples:**

The defects encountered during flowforming of Al2014 were similar to those obtained during flow forming of Al7075 and Al6101 samples. The most common defects were roller marks, wrinkling, Ovality, diametral growth, crack formation.

Figure 4.60: Defects in flow formed Al2014 product.

4.3.7.1 Crack formation in Al2014 samples

The sample for the SEM had been taken from the cracked region. A small transverse section had been cut out and the SEM image of the cracked region was investigated. The SEM image shows the morphology much different than the other samples. The morphology shows presence of microvoids and secondary particles that would have formed due to decohesion. Presence of crack can also be seen. Absence of any dimple suggests very poor ductility of the sample.

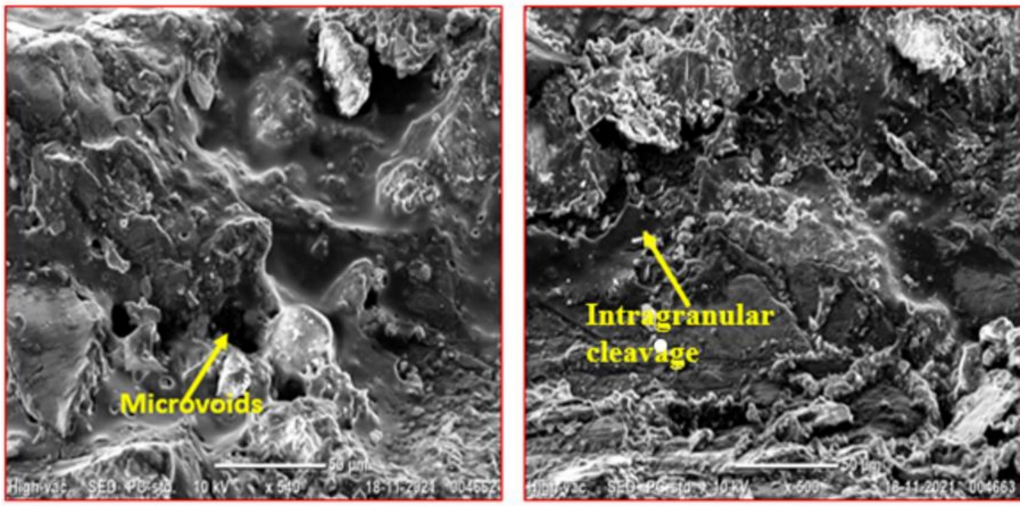

(a) (b)

Figure 4.61: Fractograph of Al2014 T6 flow formed sample at two different positions

4.4 Fractography analysis of tensile test specimen

The table shows the fractured tensile specimen of eight samples. The sample belongs to Al6101, Al7075 and Al2014 material.

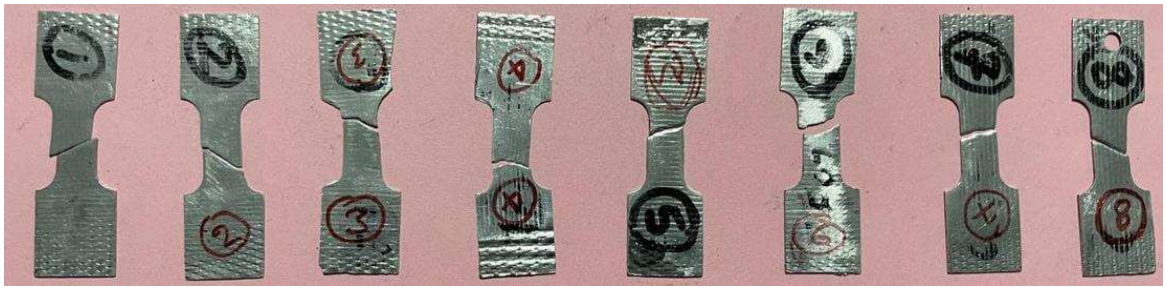

Figure 4.62: Tensile specimen after failure.

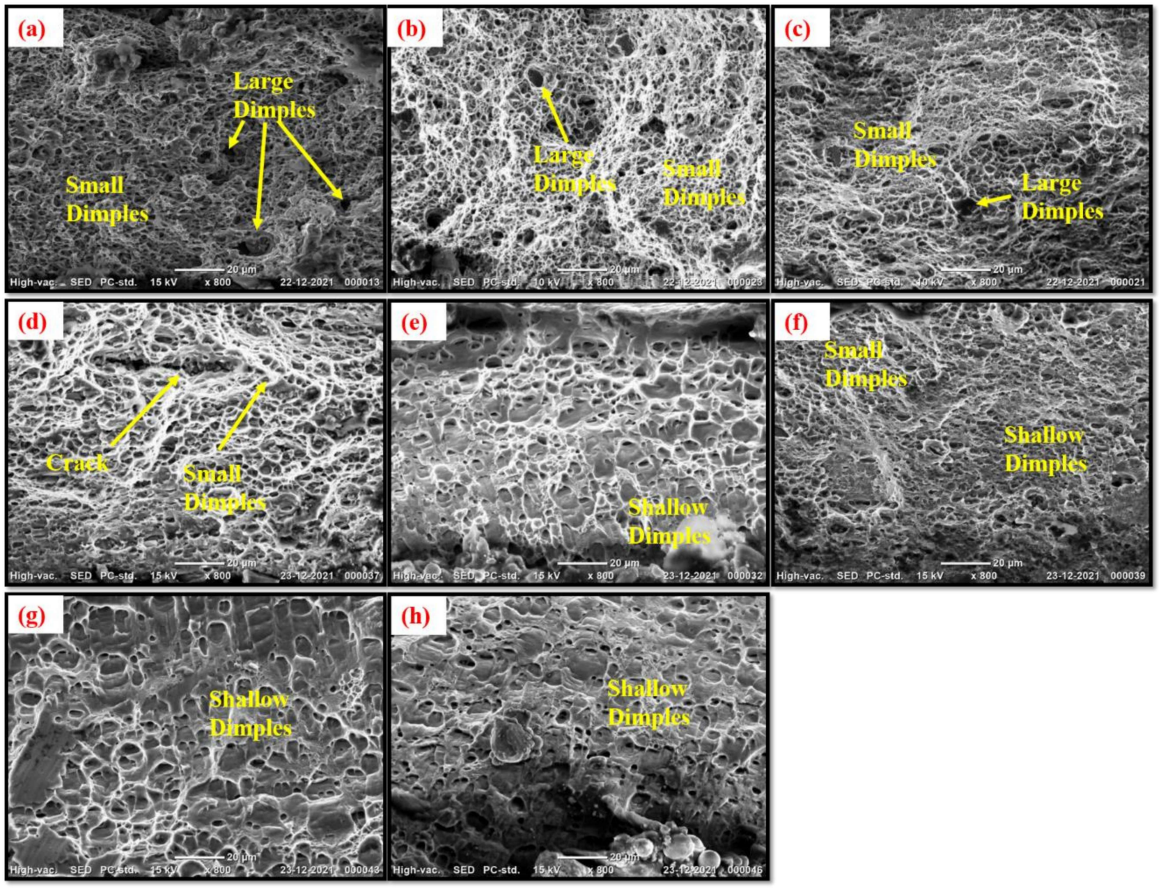

Figure 4.63: SEM fractograph (a) Al6101 T6 + flow formed (FF04) (b) Al6101 not flow formed (c) Al7075 as received material in T6 condition, heated at 470ºC for 3 hours and furnace cooled and not flow formed (d) Al7075 as received material in T6 condition, heated at 470ºC for 3 hours and furnace cooled and flow formed (e) Al7075 heat treated +flow formed (7F03) (f) Al7075 heat treated +flow formed (7F04) (g) 2014-F04 ; Al2014 heat treated + flow formed (h) Al2014 heat treated but not flow formed.

All the SEM fractographs shown in Figure 4.63 show dimple formation which indicates ductile mode of fracture. However, the morphology of dimples and their distribution shows different extent of ductility. The fraction of large dimples is more in case of Figure 4.63(b) in comparison to Figure 4.63(a). Therefore, the ductility of material shown by Figure 4.63(b) is more than the material represented by the fractograph Figure 4.63(a). Figure 4.63(c) shows both large dimples and the small dimples. However, the fraction of larger dimple is small showing lower ductility of Al7075. In Figure 4.63(d), a crack is also observed. Figure 4.63(e) and Figure 4.63(f) shows large number of shallow dimples as compared to Figure 4.63(c) showing the deformed material have lower ductility and formability as compared to preform. Figure 4.63(g) and Figure 4.63(h) shows the fractograph of Al2014. Both the fractographs shows shallow dimples showing less ductility. However, Figure 4.63(g) shows shallower features with skid surface showing lesser formability of flow formed samples.

The present chapter have presented all the results of the investigations. In the next chapter, detailed discussions on the results reported in the current chapter will be presented.